Fault rock lithologies and architecture of the central Alpine fault, New Zealand, revealed by DFDP-1 drilling

Virginia G. Toy[1], Carolyn J. Boulton[2,5], Rupert Sutherland[3,4], John Townend[4], Richard J. Norris[1], Timothy A. Little[4], David J. Prior[1], Elisabetta Mariani[5], Daniel Faulkner[5], Catriona D. Menzies[6], Hannah Scott[1], and Brett M. Carpenter[7]

[1]DEPARTMENT OF GEOLOGY, UNIVERSITY OF OTAGO, P.O. BOX 56, DUNEDIN 9054, NEW ZEALAND
[2]GEOLOGICAL SCIENCES, UNIVERSITY OF CANTERBURY, PRIVATE BAG 4800, CHRISTCHURCH 8140, NEW ZEALAND
[3]GNS SCIENCE, P.O. BOX 30-368, LOWER HUTT 5040, NEW ZEALAND
[4]SCHOOL OF GEOGRAPHY, ENVIRONMENT, AND EARTH SCIENCES, VICTORIA UNIVERSITY OF WELLINGTON, P.O. BOX 600, WELLINGTON 6140, NEW ZEALAND
[5]SCHOOL OF ENVIRONMENTAL SCIENCES, UNIVERSITY OF LIVERPOOL, LIVERPOOL L69 3GP, UK
[6]OCEAN AND EARTH SCIENCE, NATIONAL OCEANOGRAPHY CENTRE SOUTHAMPTON, UNIVERSITY OF SOUTHAMPTON WATERFRONT CAMPUS, EUROPEAN WAY, SOUTHAMPTON SO14 3ZH, UK
[7]ISTITUTO NAZIONALE DI GEOFISICA E VULCANOLOGIA, ROME 1 SECTION, VIA DI VIGNA MURATA, 605, ROME, 00143, ITALY

ABSTRACT

The first phase of the Deep Fault Drilling Project (DFDP-1) yielded a continuous lithological transect through fault rock surrounding the Alpine fault (South Island, New Zealand). This allowed micrometer- to decimeter-scale variations in fault rock lithology and structure to be delineated on either side of two principal slip zones intersected by DFDP-1A and DFDP-1B. Here, we provide a comprehensive analysis of fault rock lithologies within 70 m of the Alpine fault based on analysis of hand specimens and detailed petrographic and petrologic analysis. The sequence of fault rock lithologies is consistent with that inferred previously from outcrop observations, but the continuous section afforded by DFDP-1 permits new insight into the spatial and genetic relationships between different lithologies and structures. We identify principal slip zone gouge, and cataclasite-series rocks, formed by multiple increments of shear deformation at up to coseismic slip rates. A 20–30-m-thick package of these rocks (including the principal slip zone) forms the fault core, which has accommodated most of the brittle shear displacement. This deformation has overprinted ultramylonites deformed mostly by grain-size-insensitive dislocation creep. Outside the fault core, ultramylonites contain low-displacement brittle fractures that are part of the fault damage zone. Fault rocks presently found in the hanging wall of the Alpine fault are inferred to have been derived from protoliths on both sides of the present-day principal slip zone, specifically the hanging-wall Alpine Schist and footwall Greenland Group. This implies that, at seismogenic depths, the Alpine fault is either a single zone of focused brittle shear that moves laterally over time, or it consists of multiple strands. Ultramylonites, cataclasites, and fault gouge represent distinct zones into which deformation has localized, but within the brittle regime, particularly, it is not clear whether this localization accompanies reductions in pressure and temperature during exhumation or whether it occurs throughout the seismogenic regime. These two contrasting possibilities should be a focus of future studies of fault zone architecture.

LITHOSPHERE doi:10.1130/L395.1

INTRODUCTION

Characterizing the internal structures of major fault zones is an important step toward understanding the gross physical attributes of geological faults, including their mechanical, seismic, and hydraulic properties. Many studies have addressed this topic, and our view of fault zone structure associated with major, crustal-scale faults has developed substantially in recent years (e.g., Chester and Logan, 1986; Ben Zion and Sammis, 2003; Faulkner et al., 2003, 2008; Wibberley and Shimamoto, 2003; Holdsworth et al., 2011). These and other studies have typically revealed that deformation is distributed across a zone several hundred meters in width with varying degrees of localization. Some faults exhibit a relatively simple architecture with a single principal slip zone surrounded by a fracture damage zone, whereas others, including the San Andreas fault, contain a number of principal slip zones that in some cases anastomose and intersect, containing layers or lenses of variably fractured protolith.

These studies have contributed greatly to our understanding of the ways in which variations in rock properties influence the distribution of strain in the brittle regime. However, in the case of dip-slip faults, any particular fault rock assemblage reflects the cumulative effects of deformation occurring at a range of depths and thus under different pressure and temperature conditions. Displacement profiles across a single fault structure at a range of depths (or pseudodepths) are required to determine the three-dimensional geometry of brittle deformation. Such profiles could be acquired by constraining pressure and temperature at different times in the formation of brittle structures based on mineralogical analysis of a single, continuously exhumed crustal section, or by making observations of the structures present at a range of depths on a single large-scale structure sampled at the surface and in boreholes.

Drilling into the Alpine fault zone in the central South Island of New Zealand has recently provided the opportunity to observe a complete section across this major plate-bounding fault zone (Sutherland et al., 2012). Dextral-oblique displacement at 27 ± 5 mm yr^{-1} on the Alpine fault (Norris and Cooper, 2001) represents ~70% of the 38 ± 2 mm yr^{-1} of relative motion between the Pacific and Australian plates (DeMets et al., 2010). Rapid transport along the moderately inclined fault plane results in surface exposures of fault rocks that experienced ductile midcrustal conditions only 1–2 m.y. previously (Little et al., 2005; Norris et al., 1990). Thus, the exhumed fault rocks can be used to document the structure of the plate boundary, fault zone processes, and deformation mechanisms occurring in the midcrust in the context of a relatively simple geological and geophysical setting (Townend et al., 2009). Alpine

fault rocks have been described previously from composite sections assembled from outcrops in streams and rivers that expose the fault, but the footwall assemblage is poorly exposed (Norris and Cooper, 2007; Reed, 1964; Sibson et al., 1979, 1981; Toy, 2008; Toy et al., 2008, 2010, 2011, 2012, 2013).

The Deep Fault Drilling Project (DFDP) was established to provide new insight into the current state, seismological behavior, and geological evolution of the central Alpine fault (Townend et al., 2009), which is inferred to be late in its 200–400 yr earthquake cycle (Sutherland et al., 2007; Berryman et al., 2012). The first phase of the project, DFDP-1, was completed in early 2011 with the successful drilling, logging, and instrumentation of two boreholes intersecting the fault at depths of ~91 m and ~128 m at Gaunt Creek (Sutherland et al., 2011, 2012). DFDP-1 collected the first continuous set of rock cores, wireline geophysical logging data, and in situ hydraulic properties through the Alpine fault (Sutherland et al., 2012; Townend et al., 2013). Of particular value is the continuous nature of the recovered core, which provides a more continuous sample of lithologies immediately surrounding the principal fault slip zone than can be recovered from surface outcrop, and it has not been subject to subaerial weathering.

In this paper, we describe the fault rocks intersected in the DFDP-1 boreholes, within ~70 m of the fault's principal slip zone, based on observations of ~130 m of core and 25 thin sections representative of a larger suite of sections from samples spaced at ~0.5 m intervals throughout the core. We classify the fault rocks into eight lithological units on the basis of mineralogy and tectonite fabrics. The fault rock sequence reflects the operation of multiple overprinting deformation mechanisms and alteration processes, as pressure, temperature, and fluid chemistry evolved during exhumation. We analyzed the distribution of fault rocks within a 20–30-m-thick fault core (defined as the zone in which most fault displacement has accumulated and which contains one or more principal slip zones; Chester and Logan, 1986; as set out formally by Caine et al., 1996) and broader damage zone (defined as a zone containing low-shear-displacement structures generated during fault slip; Caine et al. 1996). In each of these zones, the rock mass has distinctive properties representing its cumulative evolution. It is these properties that likely govern the fault's mechanical response to interseismic, coseismic, and postseismic strain accommodation.

TECTONIC AND GEOLOGICAL SETTING

The Alpine fault extends on land for 600 km in the western South Island, from the southern end of the Marlborough fault system (Hope, Clarence, Awatere, and Wairau faults) to the Puysegur subduction zone in the south (Fig. 1). In the central South Island, the Alpine fault accom-

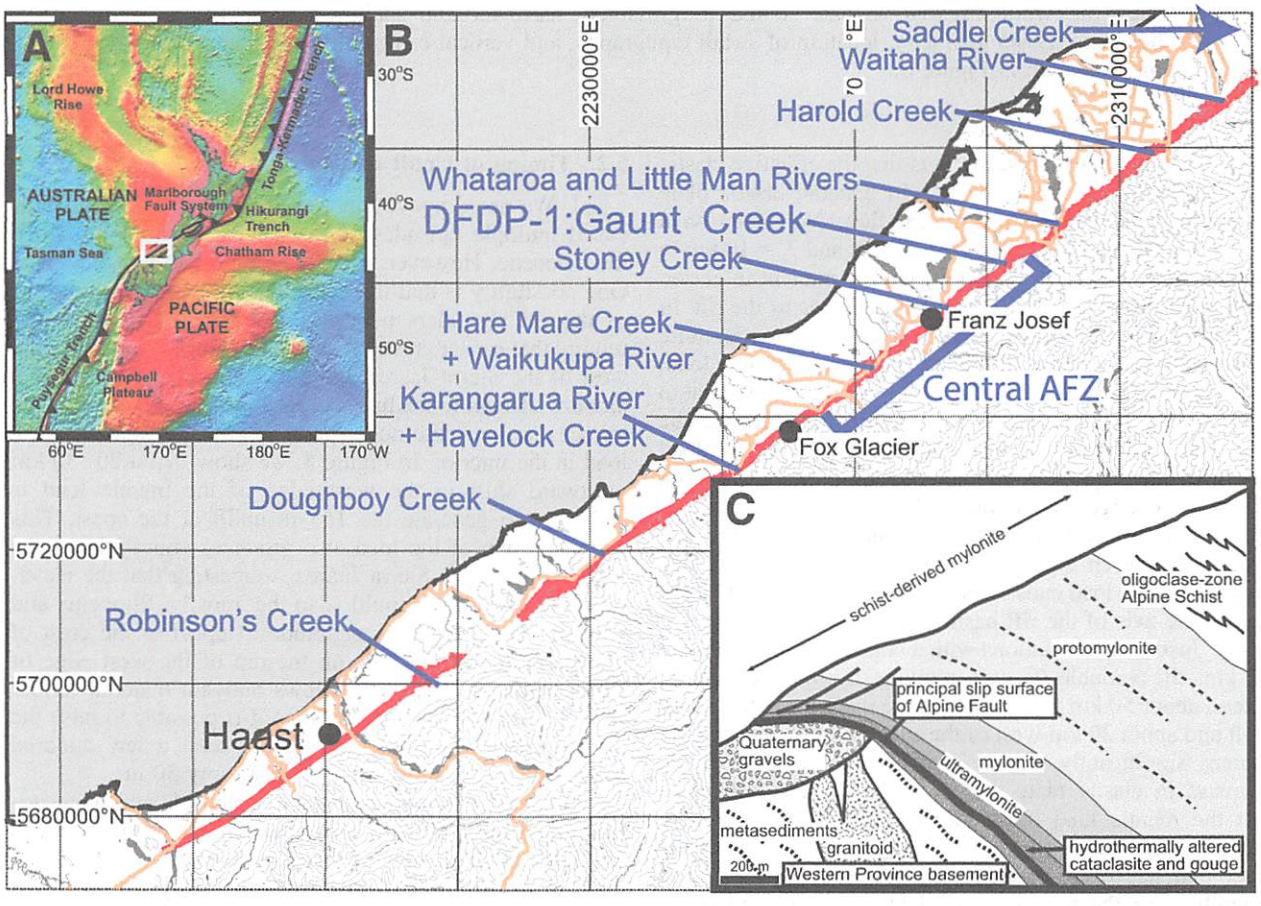

Figure 1. Location map. (A) Key tectonic elements of the Pacific-Australian plate boundary, including the Alpine fault through the continental South Island of New Zealand. Topography is after Sandwell and Smith (1997). White box illustrates location of B. (B) More detailed map of the Alpine fault (red line), illustrating locations mentioned in the text. Orange lines are roads; gray lines are topographic contours. (C) Composite schematic section through a typical Alpine fault oblique thrust segment, illustrating the sequence of fault rocks exposed in the hanging wall, modified after Norris and Cooper (2007). Outcrops at Stoney Creek, Hare Mare Creek/Waikukupa River, and Havelock Creek are particularly characteristic. DFDP—Deep Fault Drilling Project.

modates oblique-reverse slip on a moderately southeast-dipping plane that penetrates into the lower crust (Davey et al., 2007; Norris et al., 1990; Okaya et al., 2007). It is the primary plate boundary structure, with secondary faulting distributed mostly to its southeast (Cox and Barrell, 2007; Cox and Sutherland, 2007).

Regional exhumation rates in central South Island are highest between the Whataroa and Karangarua Rivers, near the DFDP-1 drill site (Fig. 1), where radiometric ages indicate that the Pacific Plate hanging wall is being exhumed at long-term rates of 6–9 mm yr^{-1} from depths of as much as 35 km (Little et al., 2005) and geodetic measurements indicate a maximum interseismic hanging-wall uplift rate of ~4 mm yr^{-1} (Beavan et al., 2007). Rapid exhumation is inferred to result in upward advection of isotherms in the hanging wall and near the fault (Koons, 1987). Microthermometric data from fluid inclusions suggest a geothermal gradient of at least 40 °C km^{-1} above the brittle-ductile transition (Toy et al., 2010), and a geothermal gradient of 63 ± 2 °C km^{-1} has been measured in the DFDP-1B borehole (Sutherland et al., 2012). This is more than double the footwall gradient nearby (Townend, 1999), and thus qualitatively consistent with the Koons (1987) model.

Plate motions in southern New Zealand have not changed significantly since 5 Ma (Cande and Stock, 2004), and there is evidence for rapid sedimentation on the footwall caused by exhumation of the hanging wall throughout that time interval (Sutherland, 1996). It is reasonable to presume, therefore, that kinematic and thermal conditions within the Alpine fault at depth have not changed during the last 5 m.y., implying that the fault rocks have formed under conditions and kinematics similar to those that currently exist at depth. The freshly exhumed material provides a globally rare opportunity to examine the structural characteristics of an active dextral-oblique fault zone, determine the deformation mechanisms active at different positions within the fault zone, and assess how and why the mechanical behavior facilitates localization of shear (Townend et al., 2009).

Geodetic measurements and observations of contemporary structures (roads, buildings, fences, etc.) and river terraces indicate that the central Alpine fault is presently locked and does not creep; however, paleoseismic evidence shows the fault to have produced large or great (M_w > 8) earthquakes in the recent geological past (Sutherland et al., 2007). From stratigraphic records of Alpine fault earthquakes at Hokuri Creek (~200 km southwest of DFDP-1), Berryman et al. (2012) determined a recurrence interval of 329 ± 68 yr. The last earthquake on the central Alpine fault was in A.D. 1717 (Howarth et al., 2012; Wells et al., 1999); present-day seismicity is diffuse and of low magnitude ($M_L \leq$ 2.5; Boese et al., 2012). Trenching of the Alpine fault scarp close to the DFDP-1 drill site indicates Holocene movement and is consistent with a last rupture in A.D. 1717 (De Pascale and Langridge, 2012). Tectonite fabrics in the fault rocks must therefore at least partially develop during earthquake-generating slip.

PREVIOUS WORK ON ALPINE FAULT ROCKS

The Alpine fault rock sequence was first described by Reed (1964) based on observations made on outcrops at Saddle Creek in the upper Kokatahi Valley, ~70 km northeast of the DFDP-1 site. Sibson et al. (1979, 1981) presented more comprehensive descriptions based on observations at many sites along strike of the fault section between Saddle Creek and Haast (~120 km southwest of DFDP-1). During the 1980s and 1990s, an extensive fault zone mapping program was undertaken by faculty and postgraduate students from the Department of Geology, University of Otago; this research and allied studies by students and faculty at other universities enabled the construction of a conceptual composite section through Alpine fault–related rocks presented by Norris and Cooper (2007).

In the central South Island (Fig. 1; typical outcrops are found at Gaunt Creek, Hare Mare Creek, Havelock Creek), the Alpine fault rocks comprise an ~1-km-thick sequence of protomylonites, mylonites, and ultramylonites derived from the adjacent Alpine Schist (Cox and Barrell, 2007), which in turn structurally overlie cataclasites and cohesive but uncemented basal gouges (Reed, 1964; Sibson et al., 1979, 1981; Warr and Cox, 2001; Norris and Cooper, 2007; Toy et al., 2010, 2011, 2012, 2013; Boulton et al., 2012). Footwall-derived rocks are present in DFDP-1, but they are rare in outcrop.

To provide a framework for DFDP-1 borehole observations, we summarize previously published descriptions of Alpine fault units in Appendix 1.

ROCK UNIT DEFINITION IN DFDP-1 BOREHOLES

In early 2011, two vertical boreholes (DFDP-1A, ~100 m depth; DFDP-1B, ~152 m depth) were drilled at Gaunt Creek using exploration diamond coring techniques (Sutherland et al., 2012). Gouges interpreted to delineate active and relict principal slip zones (PSZ) were intercepted at 90.75 m in DFDP-1A, and 128.1 m and 143.85 m in DFDP-1B (PSZ-1 and PSZ-2, respectively). We retrieved core (e.g. Fig. 2) from ~31% and ~36% of the total drilled depth in DFDP-1A and DFDP-1B, respectively, but core recovery was close to 100% near the principal slip zone surfaces. Further information regarding the technical operations, core recovery, and core processing procedures during DFDP-1 are provided in Appendix 2 and were documented extensively in the borehole completion report (Sutherland et al., 2011).

Core sections were imaged using a Geotek multisensor core logger (MSCL), which involved taking photographs from three different angles and then stitching these images together to produce unrolled images (e.g., Fig. 3). Mineralogical and microstructural characterization was undertaken on samples spaced at intervals of ~0.5 m throughout both DFDP-1A and DFDP-1B cores. Polished thin sections were examined using standard optical microscopy. Some of the fault rocks are very fine grained; thus, microstructural and chemical characterization required backscattered electron images, which were obtained on a Zeiss Sigma VP FEG (field emission gun) scanning electron microscope.

Lithological Descriptions and Structural Interpretation of Rock Units Identified in DFDP-1

We distinguished eight rock units in the DFDP-1 boreholes: gray and dark-green ultramylonites; brown-green-black ultramylonites; upper unfoliated cataclasites; upper foliated cataclasites; gouges; lower cataclasites; breccias; and Quaternary gravels (not further described herein). We have defined these units such that they can be distinguished at hand-specimen scale, and we have placed particular emphasis on distinctive mineralogical compositions, colors, and tectonite fabrics (summarized in Table 1). Our fault rock nomenclature follows that of Woodcock and Mort (2008). Units are numbered sequentially in the order they were encountered from top to bottom of the recovered core. The distribution of these rock units, compiled from the full suite of comprehensive core logs, is presented in Figure 2, and Figure 3 illustrates representative sections of core within each lithology. Typical microstructures of the units are illustrated in Figures 4–6. Basic descriptions of the characteristic mineralogy, microstructure, and fabric for each unit are presented in Table 1. Results are based on a combination of thin-section observations and qualitative X-ray diffraction (XRD) analysis of samples from the finest-grained materials, as described in detail elsewhere (Boulton, 2013).

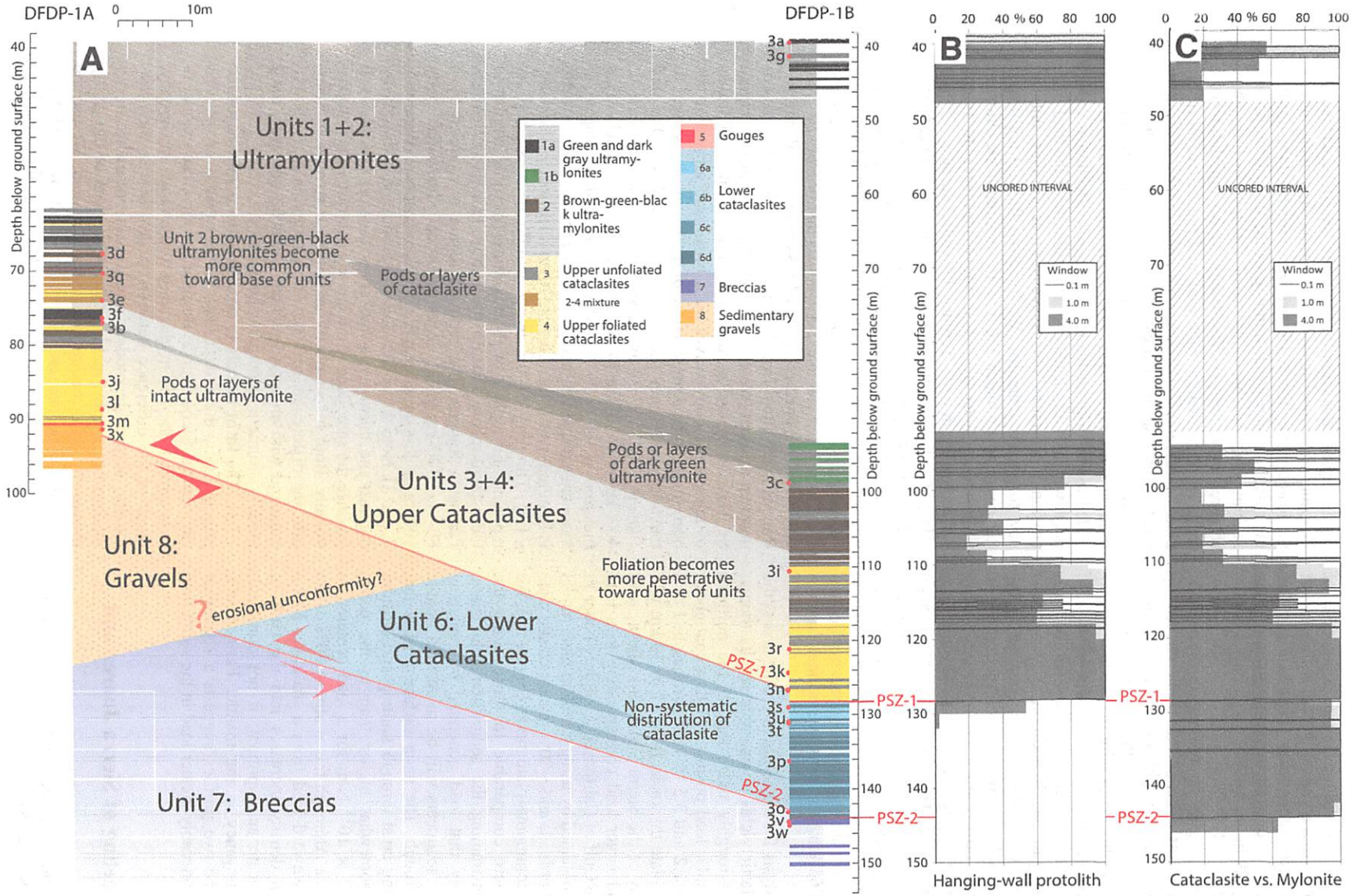

Figure 2. (A) Summary lithological columns from Deep Fault Drilling Project (DFDP) boreholes DFDP-1A and DFDP-1B, illustrating distribution of the various lithological units as interpreted from core logs. Uncolored intervals are those where no core was recovered. Units have been correlated between the two boreholes. Red dots indicate positions of core scans illustrated in Figure 3. (B–C) Illustration of affiliation of the units to (B) hanging wall (units 1, 3, 4) as opposed to possible footwall (units 2, 6, 7 in DFDP-1B) and (C) cataclasite (units 3, 4, 6) or mylonite (units 1, 2, 7). These were constructed using moving window averages with window "widths" as indicated in the key; horizontal scale is the percentage of recovered core within that window that is composed of any one of the lithological units included in that category. These points are plotted at twice the density of the window within which they are averaged (e.g., for a 1 m window, the average has been calculated at 49.0 m, 49.5 m, 50.0 m, etc.). PSZ—principal slip zone.

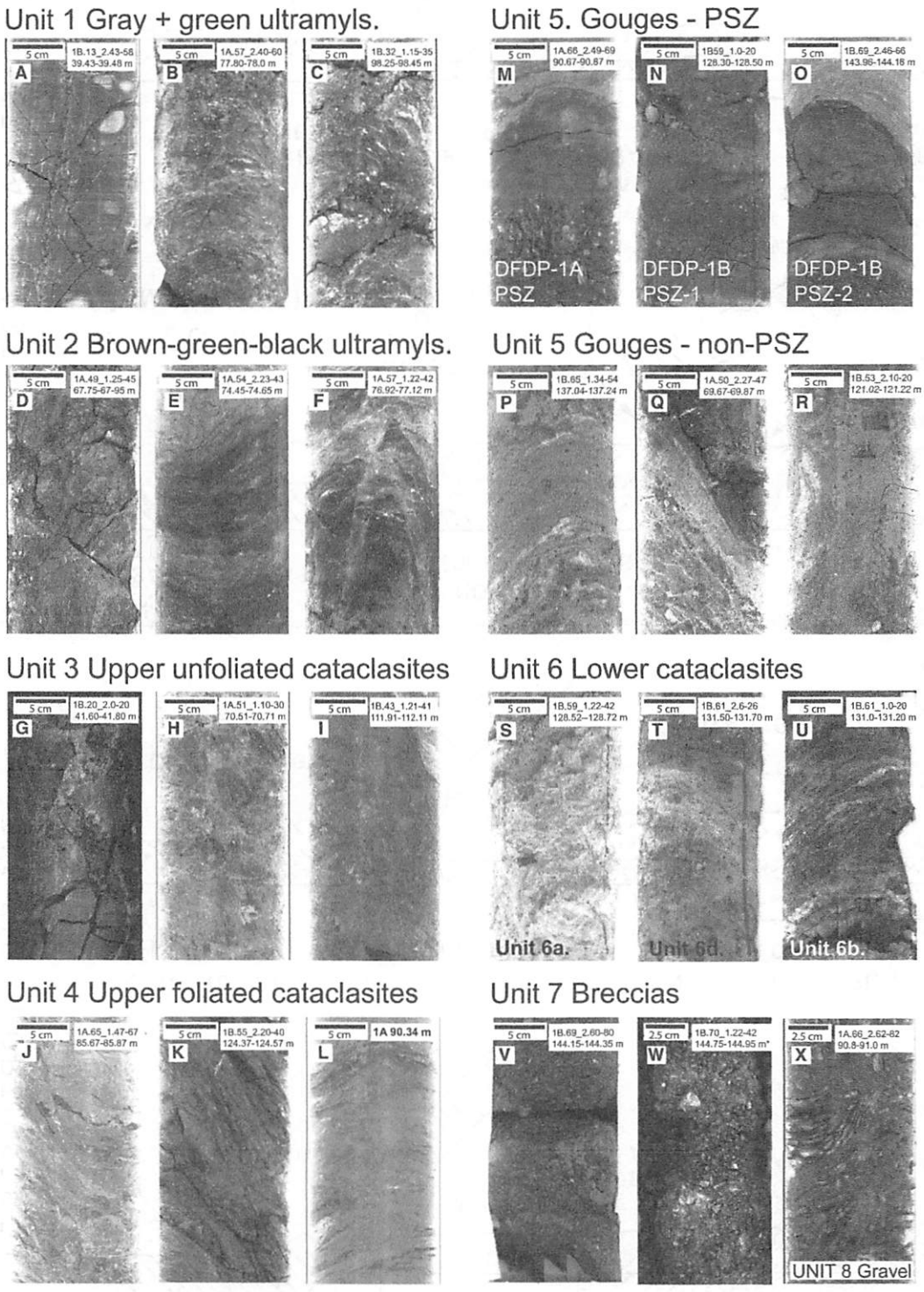

Figure 3. Unrolled 180° scans (5 cm scale bars) or flat scanned images (2.5 cm scale bars) of core sections typical of the various lithological units. Comprehensive descriptions of each unit are provided in Table 1. Notable features within these scans include (A) steep trains of feldspar augen and later crosscutting fractures; (B) spaced foliation; (C) discontinuous foliation-parallel quartz veins; (D) steep and shallow foliations; (E) oblique foliations and disjunctive cleavage; (F) late, high-angle conjugate gouge-bearing faults; (G) recemented breccia; (H) remnants of mylonitic foliation at top right; (I) all mylonitic foliation destroyed; yellow (Fe-carb?) veins; (J) remnant dark-gray–green ultramylonite layering; (K) disjunctive cleavage; (L) highly comminuted end member; (M) unit 8 sedimentary gravel (base of image); (N–O) principal slip zone (PSZ) gouges: (N) centimeter-scale layers of different grain sizes and disaggregated fragment of calcite vein (arrowed); (O) upper and lower margins of this particular gouge layer that are not parallel; (P–R) layer boundaries that mostly parallel fabrics in bounding cataclasites in gouges not identified as principal slip zones; (S–U) the broad range of appearances of the lower cataclasites (remnant gneissic layering is very obvious in part U); (V–W) the typically uncemented nature of unit 7 breccia; and (X) foliations, which are revealed where clasts in the gravel were dissected during coring. DFDP—Deep Fault Drilling Project.

TABLE 1. CHARACTERISTIC FEATURES OF LITHOLOGICAL UNITS ENCOUNTERED IN DEEP FAULT DRILLING PROJECT (DFDP-1)

Unit number	Name	General lithology	Mineralogy and grain sizes	Fabric and microstructure	Notes
1	Gray and dark green ultramylonites	1a. Planar-foliated, medium-gray (N5) to medium dark-gray (N4) quartzofeldspathic, mostly oligoclase-bearing ultramylonites. 1b. Planar-foliated, dark greenish gray (5GY 4/1) metabasic, mostly oligoclase-bearing ultramylonites.	Quartz + oligoclase + biotite + muscovite ± calcite ± chlorite + accessories. Grains mostly ≥30 μm and range up to millimeters long. Quartz + oligoclase + biotite + hornblende ± muscovite ± calcite ± epidote ± chlorite + accessories. All grains ≥30 μm and range up to millimeters long.	Millimeter- to centimeter-long quartz + feldspar versus mica/amphibole-rich segregations (Fig. 3B), aligned mineral long axes and locally abundant feldspar augen trains (Fig. 3A) define a smooth, millimeter-spaced to continuous foliation (S). Transition from spaced (Fig. 4B) to continuous foliation (Fig. 4A) occurs with increasing strain. S surfaces are transected by C′ shear bands (Figs. 4A and 4B). In unit 1b., spaced felsic-amphibole layering (Fig. 4B) and continuous foliations are observed with no systematic relation to position in the fault zone. Quartz grains have undulose extinction and interlobate grain boundaries (arrowed Fig. 4A).	1a. is medium to dark gray (locally black) and 1b. is dark green. This color division reflects original protoliths. The overall protolith for unit 1 is almost certainly the Alpine Schist subgroup of the Haast Schist, as discussed in the section entitled "Discussion of Inferred Protoliths". Bands of 1b. range from 0.1 to 2 m thick.
2	Brown-green-black ultramylonites	Planar-foliated, mixed medium dark-gray (N4), grayish black (N2), olive gray (5Y 4/1), olive black (5Y 2/1), dark greenish gray (5GY 4/1), quartzofeldspathic to metabasic, mostly albite-bearing ultramylonites.	Quartz + albite(?) + chlorite + epidote + accessories. Grains mostly <50 μm but rare feldspar porphyroclasts range <200 μm. Quartz aggregates composed of grains <10 μm.	Indistinct millimeter-spaced foliation defined by dark, hairline seams of opaques and parallel large grains of mica (sericite?) forming a locally dilatant "disjunctive" cleavage (Fig. 4C). In places, a spaced foliation is defined by brown-black bands of fine-grained quartz-feldspar-epidote-chlorite alternating with millimeter-thick bands higher in opaques and clay minerals, or quartzofeldspathic bands that are planar, or anastomosing around equant feldspar porphyroclasts. Aligned phyllosilicate foliation is also present in some of the black pods. A few dark seams are at high angle to the dominant foliation. No systematic crosscutting relationship is observed between these and the main seams; they were presumably coeval.	Distinctly finer grained than unit 1 (quartz grain sizes ~10 μm rather than ~30 μm). Microfaults at high angle to foliation commonly divide the decimeter- to meter-thick black + green layers (Figs. 2D and 2E) into fault-bounded wedges (Fig. 2F) Major-element chemistry suggests a mixture of Pacific and Australian plate protoliths (as discussed in the section entitled "Discussion of Inferred Protoliths").
3.	Upper unfoliated cataclasites	Unfoliated, pale yellowish to olive gray (5Y 8/1–5Y 4/1), greenish gray (5GY 6/1), and medium bluish gray (5B 5/1), quartzofeldspathic and rarely metabasic cataclasites.	As for units 1 and 2, with more chlorite, epidote, calcite (mostly as cements), and brown or blue-gray clay (chlorite + illite/muscovite). Matrix grains mostly <10 μm to below optical resolution, feldspar porphyroclasts <100 μm.	Angular fragments <10 cm in diameter of units 1 and 2 in a variably calcite-cemented patchy cryptocrystalline (clay) matrix (Fig. 4E). Clast-supported when fragments are >1 cm diameter (Fig. 2G); in these cases, protolith foliations are not significantly misaligned in adjacent clasts, implying minimal clast rotation, and clast:matrix ratios are mostly <0.5. Matrix-supported when clasts are finer than ~1 cm diameter (Figs. 3H and 3I); in these cases, there is evidence of significant clast rotation, and clast:matrix ratios range from 0.5 to 1.0. Rarely a foliation is defined by anastomosing, dark, hairline seams, spaced <0.2 mm (e.g., Fig. 3H).	The extent to which original intact rock has been fractured and clasts have been rotated varies so these rocks span the spectrum from "fractured protolith" to "ultracataclasite" sensu stricto (Sibson, 1977). Multiple episodes of cataclasis and calcite cementation are typically indicated by crosscutting relationships.
4.	Upper foliated cataclasites	Foliated, yellowish to olive gray (5Y 8/1–5Y 4/1), and very light-gray (N8), with seams of greenish gray to greenish black (5GY 6/1–5GY 2/1), quartzofeldspathic and rarely metabasic cataclasites.	As for units 1 and 2, with more chlorite, epidote, calcite (mostly as cements), and significant amounts of typically blue-gray clay (chlorite + illite/muscovite). Centimeter-scale quartzofeldspathic pods and salmon pink clasts/veins are present. Matrix grains mostly <10 μm to below optical resolution, feldspar porphyroclasts <100 μm.	Comprises clasts of lense-shaped, subangular feldspar or angular calcite (Fig. 4G) in a very variable proportion of clay matrix (from 0%–90%). The latter may form tabular patches (Fig. 4H). Elsewhere the matrix is comminuted feldspar, quartz, chlorite, white mica, and calcite (Fig. 5A) ± epidote (Fig. 5B) or disseminated (neomineralized?) calcite (Fig. 5B). The clast size generally decreases with proximity to the inferred principal slip surfaces; the finest-grained materials are barely cohesive and clay-rich, and equate to ultracataclasite sensu stricto (Sibson, 1977). Foliation is defined either by anastomosing dark seams (i.e., disjunctive cleavage; Figs. 3K and 6A) appearing as black hairlines on core surface and defined by opaques or clays in thin section (Fig. 4F) or by aligned phyllosilicates that may link in an anastomosing network similar to an S-C″ shear fabric (Fig. 4G), mostly appearing black on the core surface. Millimeter-scale brown-green-black bands (inherited mylonitic foliation) are also rarely preserved (Fig. 3J). Both fabrics may anastomose around lenticular fractured clasts of protolith (quartz + epidote + chlorite [Fig. 4F]; internally unfoliated quartz-feldspar [Fig. 4H]; feldspar with intragranular calcite and overgrowths [Fig. 5A]; disaggregated veins and clasts of calcite with narrow, planar e-twins [Fig. 5C, D]; quartz [Fig. 5B]). Foliation may anastomose within packages and displays both gradual and discrete (shear-bounded) changes in orientation. There are manganese and iron oxide–hydroxide cements (e.g., Figs. 5A and 5B).	No evidence for shear on solution seams. Phyllosilicate foliation inherited? Fabrics better developed with increasing depth in the core, accompany gradual color changes, suggesting change in alteration mineralogy. Black/green division has been retained from unit 2, but lenses are boudinaged and offset by centimeter-displacement faults (e.g., Fig. 2J).

(continued)

TABLE 1. CHARACTERISTIC FEATURES OF LITHOLOGICAL UNITS ENCOUNTERED IN DEEP FAULT DRILLING PROJECT (DFDP-1) (*continued*)

Unit number	Name	General lithology	Mineralogy and grain sizes	Fabric and microstructure	Notes
5.	Gouges	Foliated to unfoliated, light olive gray to olive black (5Y 6/1–5Y 2/1), with seams of greenish black (5GY 2/1) and white (N9) to very light-gray (N8) clasts, cemented to uncemented gouges.	As for units 3 and 4, but with significantly more calcite (mostly as cement), and clay (smectite + illite/muscovite ± kaolinite). Matrix grain size ≪10 μm. Clasts range <1 μm but mostly much less.	Medium brown or gray-blue clay-rich ultra-fine-grained material with a scaly fabric. Layering is indistinct; rarely, subplanar, high aspect ratio, less than centimeter-thick lenses of material with visible versus invisible particles mostly <50% define a fabric parallel to unit boundaries (Fig. 3N). Matrix includes aligned phyllosilicates with uniform extinction and amorphous iron and manganese oxide-hydroxides (Fig. 5D). The subrounded clasts include grains of calcite with narrow e-twins; fine-grained aggregates of calcite with altered (to sericite and saussurite) feldspar (Figs. 5C, 5D, and 5F); recycled ultracataclasites/gouges (Fig. 5D) with calcite cement and rarely amygdaloidal material (possible pseudotachylyte; Fig. 5F). Matrix phyllosilicates may wrap clasts ("snowball" fabric of Warr and Cox, 2001; Fig. 4D).	Typically cohesive but uncemented. Upper and lower boundaries of unit are not necessarily parallel. In PSZ-1 in DFDP-1B, the boundary with lower cataclasite has <1-mm-long flame-like injection structures.
6.	Lower cataclasites	6a. White (N9) to very light-gray (N8) and yellowish gray (5Y 8/1) granular cataclasite.	Quartz + feldspar (may be plagioclase or orthoclase) + chlorite-muscovite + clays (blue-gray; illite/muscovite) ± biotite. Grains in protolith granites and gneisses mostly >>100 μm diameter (Fig. 6). Cataclasites comprise patches of clasts <100 μm (Figs. 6G and 6C) in a matrix of grains <30 μm and rarely much larger (millimeter-scale) clasts (Fig. 6B).	Cataclasite with medium to coarse sand (0.5–1 mm) sized, subangular to subrounded qtz-feldspar clasts and matrix proportion from 0% (quite common) to >70%. The unit is poorly indurated but cohesive. Gneissic texture may be defined by elongate muscovite and quartz ribbons composed of numerous blocky, moderately equant grains (Fig. 6C). Feldspar porphyroclasts comprise microcline (note cross-hatched twins indicated by arrows in Fig. 6C). Myrmekite (Fig. 6B) and flame perthite (Fig. 6A). Rare clasts display interlocking texture of biotite-quartz-feldspar typical of granite (Fig. 6D).	Sporadic observations of feldspar and biotite in an interlocking texture strongly suggest a granitic protolith (Fig. 5D). Clast color ranges from light to dark green, black, white, and salmon pink. Granitoid and gneissic textures and high natural gamma values (Townend et al., 2013) suggest derivation from an Australian plate protolith as discussed in the section entitled "Discussion of Inferred Protoliths".
		6b. Dark greenish gray (5GY 4/1) foliated cataclasite to fractured protolith.		Distinctly layered foliated protocataclasite to cataclasite, locally retaining an ultramylonite foliation (sometimes in pods with foliation oblique to contacts with surrounding rock; Fig. 3U).	
		6c. Unfoliated dark-gray (N3) to dark greenish gray (5GY 4/1) and greenish black (5GY 2/1) clay-rich ultracataclasite to gouge.		Matrix-supported, cohesive, foliated gray to green clay-rich ultracataclasite to gouge, with clayey matrix and subrounded to subangular, coarse sand-sized (0.5–1 mm) clasts of a quartz-plagioclase-chlorite–rich protolith.	
		6d. Mixture of 6a–6c. Range of colors including those observed in 6a–6c, as well as medium dark-gray (N4) and light olive gray (5Y 6/1).		Coarse to very coarse grained with >50% cohesive matrix of comminuted K-feldspar + plagioclase + clinochlore + calcite + epidote + apatite + pyrite + muscovite (Figs. 5E and 5G). Constituent materials are either interlayered (Fig. 5F) or form fault-bounded pods. Ultra-fine-grained, clayey patches are present. Clasts include subangular to subrounded quartz + feldspar in places crosscut by calcite veins and fragmented with little clast rotation or translation (Fig. 4E).	
7.	Breccias	Unfoliated, dark greenish black (5G 2/1) breccia with remnant mylonitic foliation and white (N9) to very light-gray (N8) porphyroclasts.	Quartz + K-feldspar + amphibole + epidote + chlorite + muscovite + opaques + accessories (e.g., apatite, graphite). Matrix quartz and mica generally tens of millimeters in diameter with larger (>250 μm) feldspar porphyroclasts (Fig. 5H)	Variably cemented protocataclasite to breccia composed of angular-subangular clasts of weakly foliated black mylonite-gneiss that are either augen-bearing or contain quartz segregations. A sandy matrix, may be drilling-induced material or primary. Clasts internally have spaced foliation of quartz bands wrapping feldspar porphyroclasts. There are also phyllosilicates on porphyroclast margins. Quartz bands are subdivided into polygonal aggregates and subgrains in elongate patches with similar extinction reminiscent of stretched larger grains, and rare elongate grains with undulose extinction but no distinct subgrains (Fig. 5H).	We cannot say if brecciation is drilling-induced or tectonic.
8.	Sedimentary gravels	Color ranges from white (N9) to grayish black (N2).		Gravel composed primarily of angular to subrounded Alpine Schist clasts, ~1–10 cm diameter, in a medium sand matrix.	This unit is only present at the base of DFDP-1a as well as in the Gaunt Creek scarp and terrace exposures.

Note: Colors used in descriptions in this table accord with Munsell (1912) hues, values, and chroma, and are expressed as codes (e.g., 5N, or 5GY 4/1). These were chosen by reference to The Geological Society of America's *Rock Color Chart*, 7th printing (1991).

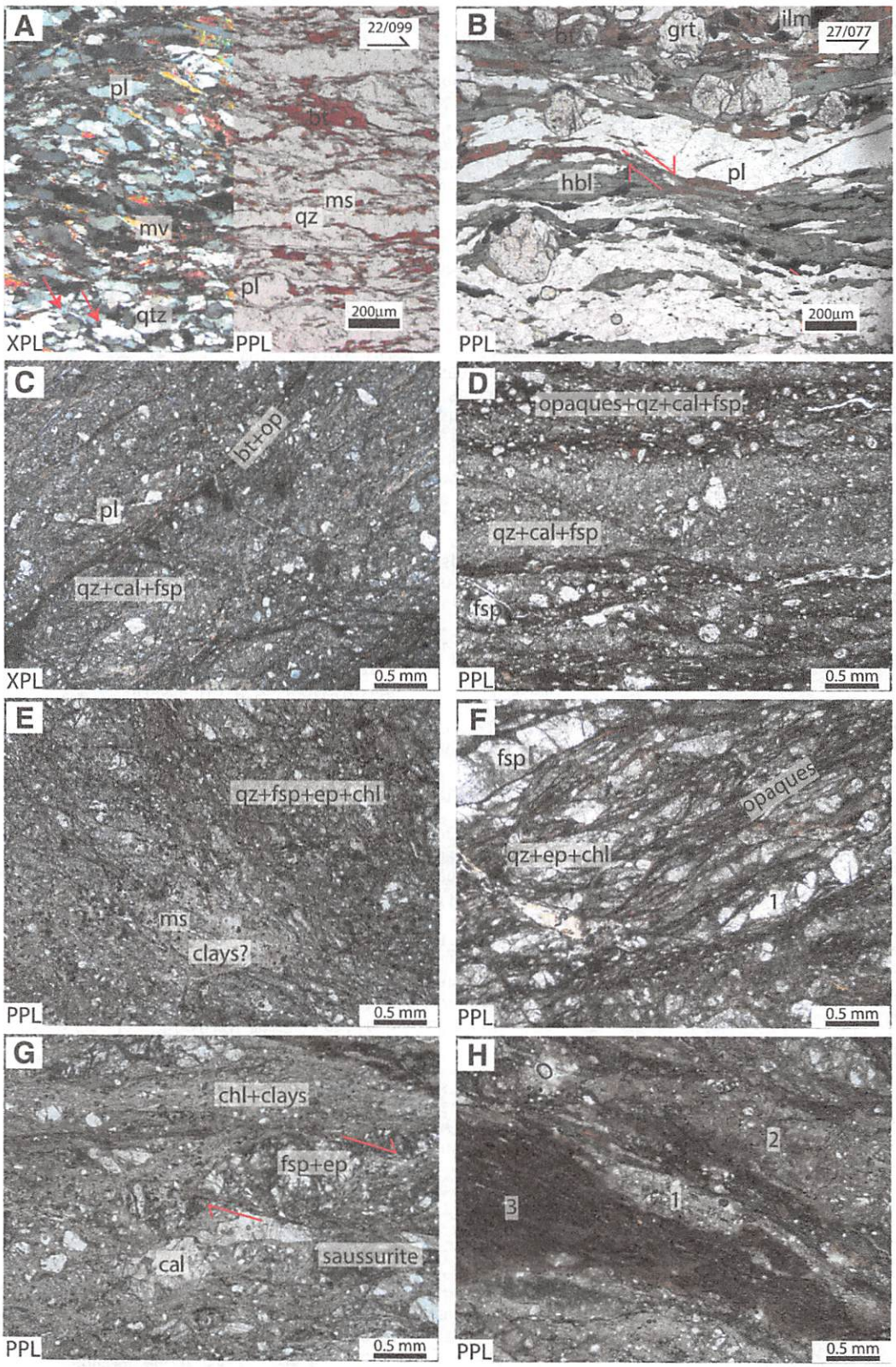

Figure 4. Optical microscope images of characteristic hanging-wall lithologies. Abbreviations for mineral labels follow Whitney and Evans (2010). PPL—plane polarized light; XPL—cross-polarized light. Arrows indicate shear senses inferred from microstructures. (A) OU77897 and (B) OU77887 are derived from outcrop adjacent to Deep Fault Drilling Project (DFDP-1) boreholes. (A) Unit 1 gray ultramylonite. (B) Unit 1 dark-green (metabasite) mylonite. (C) Unit 2 black ultramylonite, DFDP-1A, 79.72 m depth (1A.59_1.32). There are rare larger (<200 mm) feldspar porphyroclasts. (D) Transitional unit 2 black ultramylonite to unit 4 foliated cataclasite, DFDP-1A, 74.50 m depth (1A.54_CC.08). (E) Unit 3 upper unfoliated cataclasite, DFDP-1A, 79.35 m depth (1A.58_CC.05). (F) Unit 4 upper foliated cataclasite, DFDP-1A, 80.50 m depth (1A.60_1.0). (G) Unit 4 upper foliated cataclasite, DFDP-1B, 128.04 m (1B_58_1_0.90). (H) Unit 4 upper foliated cataclasite, DFDP-1B, 128.04 m (1B_58_1_0.90). In this image, three different domains within which grain size and proportion of opaques vary are numbered 1–3 in order of decreasing clast sizes and increasing proportion of clays in matrix.

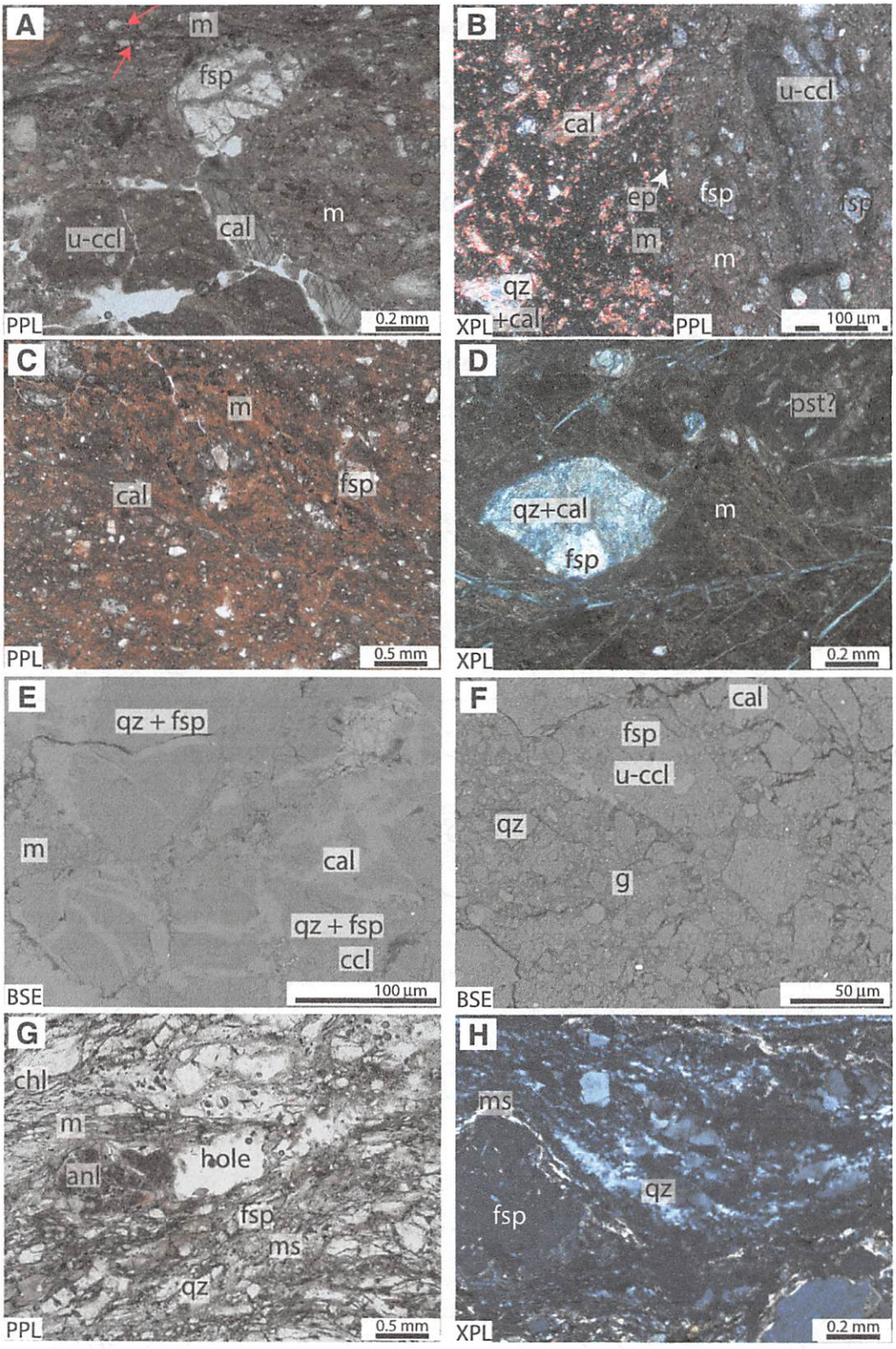

Figure 5. Optical and scanning electron microscope (SEM) images of fault core and footwall lithologies. Abbreviations for mineral labels follow Whitney and Evans (2010); additionally, m—mica, u-ccl—ultracataclasite, ccl—cataclasite, m—gouge matrix, pst—pseudotachylyte, PPL—plane polarized light, XPL—cross polarized light, BSE—backscattered electron SEM image. (A) Unit 4 foliated cataclasite to unit 5 blue gouge transition interval in Deep Fault Drilling Project (DFDP-1A), 90.36 m depth (1A.66_CC.18). Arrows indicate overgrowths on feldspar porphyroclasts. (B) Unit 5 blue gouge in DFDP-1A, 90.62 m depth (1A.66_CC.44). Both photomicrographs are of the same sample. (C) Principal slip zone (PSZ) unit 5 brown gouge in DFDP-1A, 90.70 m depth (1A.66_CC.52). (D) PSZ-1 unit 5 brown gouge in DFDP-1B, 128.44 m depth (1B_59–2_0.14). Cracks crosscutting the image formed during thin-section preparation. (E) Unit 6d mixed cataclasite immediately above an undulating contact with PSZ-2 unit 5 gouge, DFDP-1B, 144.01 m (1B_69–2_0.47). (F) PSZ-2 unit 5 gouge, DFDP-1B, 144.02 m (1B_69–2_0.48). (G) Unit 6d. Plane polarized light. (H) Clast in unit 7 breccia, DFDP-1B, 144.75 m (1B_71–2.0.55).

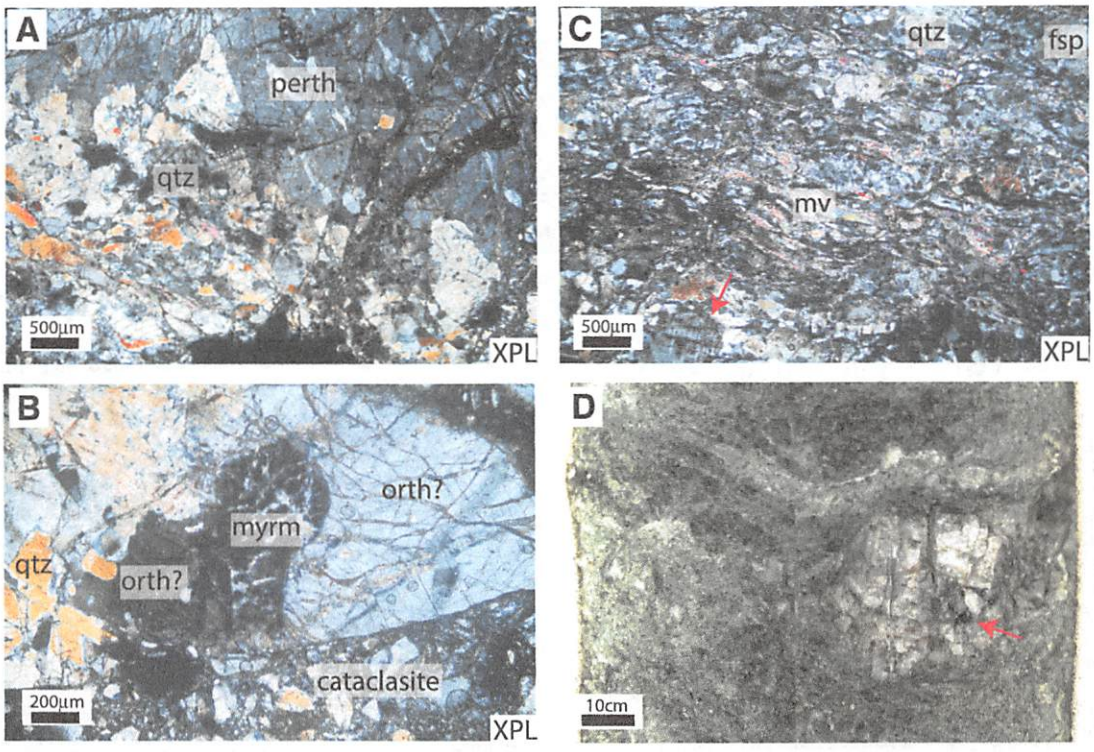

Figure 6. Photomicrographs and photographs illustrating evidence for a granitic or gneissic protolith to unit 6a "white to gray granular cataclasite" in Deep Fault Drilling Project (DFDP) borehole 1B. Abbreviations for mineral labels follow Whitney and Evans (2010); additionally, mrym—myrmekite, perth—perthite, PPL—plane polarized light, XPL—cross-polarized light. (A) 1B.61_3.0, (B) 1B.61_3.0, (C) 1B.65_2.7; note gneissic texture with foliation delineated by dashed line; (D) 1B.66_2.10–12: 180° scan of core. Red arrows highlight features particularly indicative of a granitic protolith as explained in Table 1.

INTERPRETATIONS OF DEFORMATION PROCESSES FROM CORE- TO MICROSCOPIC-SCALE OBSERVATIONS

Unit 1: Gray and Dark-Green Ultramylonites

Millimeter-spaced foliation of coarse quartz-feldspar and mica or amphibole layers is transected by shear bands (e.g., those apparent in Fig. 4B) and forms the interconnected weak layer morphology defined by Handy (1990). Quartz microstructures, such as undulose extinction, subgrains, and interlobate grain boundaries (arrowed in Fig. 4A), and undulose extinction observed in biotite, muscovite, and feldspar are typical of those observed experimentally during crystal plastic deformation (Hirth and Tullis, 1992; Mariani et al., 2006; Pryer, 1993). We infer that dislocation creep and grain-size-sensitive creep accommodated deformation within these rocks (see also Toy et al., 2013), and that this lithology mostly developed within midcrustal parts of the shear zone below the seismogenic zone.

Unit 2: Brown-Green-Black Ultramylonites

Abundant solution seams are defined by concentrations of micas and opaque minerals (e.g., Fig. 4C and 4D), and apparent pressure shadows contain quartz, epidote, and chlorite, combined with a more hydrous mineralogy than that found in other schist-derived ultramylonites (chlorite + epidote + albite + quartz as opposed to biotite + muscovite + quartz + oligoclase ± amphibole). These features suggest that pressure solution–accommodated, aseismic, grain-size-sensitive creep was an important deformation mechanism in these rocks (Gratier et al., 2011); however, pseudotachylyte patches, particularly fault veins displaying mutual cross-cutting relationships with other brittle structures, are also common in this unit (arrowed in Fig. A2D), indicating that slip rates were episodically high (Cowan, 1999; Sibson and Toy, 2006; Toy et al., 2011). We conclude that this unit records a fluctuation in deformation mechanisms as slip rates varied between aseismic and seismic slip.

Unit 3: Upper Unfoliated Cataclasites

The random fabric results from numerous mutually overprinting brittle events, manifest as decimeter- to centimeter-scale faults (macroscopically visible in Fig. 3G and Fig. A2G–A2I, where they are highlighted by yellow arrows). Crosscutting relationships and the general abundance of hydrous minerals (mica, chlorite) and calcite, which commonly precipitate from solution, illustrate a complex history of brittle failure and fluid migration likely accompanying deformation. Anastomosing solution seams are also observed microscopically (Fig. 4E), suggesting some deformation was accommodated by pressure solution–accommodated grain-size-sensitive creep (Gratier et al., 2011). The lack of penetrative foliation in this unit indicates that brittle frictional deformation mechanisms predominated (Sibson, 1977). This is most likely in quartzofeldspathic crust at temperatures less than 300 °C (Voll, 1976; Stöckhert et al., 1999; Tullis, 2002) in the seismogenic portion of the fault zone. In addition, the predominance of illite/muscovite and chlorite (as opposed to the smectite found in unit 5; see following) suggests that much of

the cataclastic fabric formed toward the deeper part of the seismogenic zone, as smectites are thermally unstable above ~150 °C (Inoue and Utada, 1991; Moore and Reynolds, 1997).

Unit 4: Upper Foliated Cataclasites

In this unit, foliation planes defined by thin (<1 mm) layers of opaque minerals or clay-sized phyllosilicate grains are most common near the principal slip zone (within <10 m; Figs. 3K and 3L). Opaque phases are concentrated in seams interpreted to result from preferential solution of less-soluble minerals (e.g., Gratier et al., 2011). Once formed, these structures may have accommodated some shear, as they bound asymmetric porphyroclasts (e.g., Fig. 4F). More prominently, phyllosilicate foliations wrap around competent polycrystalline clasts and provide further evidence for shear (e.g., feldspar + epidote clast in Fig. 4G). We infer that deformation of foliated cataclasite occurred at subseismic slip rates, based on comparisons with the deformation of synthetic fault gouges in which phyllosilicate-rich foliations are produced as a result of dissolution-diffusion-precipitation processes at low strain rates (Niemeijer and Spiers, 2005). However, the absence of internal foliation in quartz- and feldspar-rich layers (Fig. 4H) suggests that they were deformed at stresses high enough to fracture grains and/or at higher strain rates, as inferred for the generation of unit 3 upper unfoliated cataclasites. These mixed textures likely indicate that throughout its evolution, the rock was deformed at a range of strain rates. The mineralogy of this unit is comparable to that of unit 3, again suggesting that deformation occurred in the deeper parts of the seismogenic zone.

Unit 5: Gouges

In the nearby outcrop, cohesive but uncemented gouge can be clearly identified as marking the principal slip zone because it separates cataclasite from late Quaternary gravel (Cooper and Norris, 1994; see also Toy and Mitchell, 2014). The very fine-grained nature of this gouge, a consequence of ultracomminution, and presence of recycled gouge clasts indicate that it formed during multiple increments of shear under brittle conditions (Boulton et al., 2012). We identified a similar gouge to that described by Boulton et al. (2012) in the DFDP-1A borehole at 90.75 m depth, and we note that it has distinctively different geophysical properties (particularly low resistivity, density, and P-wave velocity, and high spontaneous potential) from those of other rocks in the borehole (Townend et al., 2013).

In the DFDP-1B borehole, similar gouges occur at two distinct depths: 128.1 m (PSZ-1) and 143.85 m (PSZ-2). These separate: (1) a similar unit 4 foliated cataclasite to that found in DFDP-1A from a more diverse cataclasite beneath, which has greater feldspar and quartz content (unit 6), and (2) a unit 6 cataclasite from a unit 7 angular breccia. In addition to recycled gouge clasts similar to those observed by Boulton et al. (2012; their Figs. 4a, 4b, 4f), we observed rare clasts of likely pseudotachylyte within the gouge (Fig. 5D) and a predominantly random fabric (prominent in Fig. 5F).

We have not observed continuous, undeformed pseudotachylyte in the principal slip zone gouge, so we cannot say frictional melting occurred during the final increment of seismic slip in this material. However, the average grain size within the gouge clasts (which are distinct from matrix due to color or foliation attitude) is comparable to that of the matrix and is always substantially finer than observed in surrounding cataclasite units, which strongly supports the interpretation that they are only reworked from within this material. We infer this is also the case for pseudotachylyte clasts, and, thus slip, at least locally, occurred at seismic rates on or near the principal slip zone (Sibson, 1975). Conversely, there are also phyllosilicate foliations (e.g., Figs. 5C and 5D) that wrap the recycled clasts and thus cannot be inherited from the protolith mylonite. By analogy to the work of Niemeijer and Spiers (2005) and Rowe et al. (2011), these may have formed during increments of aseismic creep. Where phyllosilicates wrap around clasts (Fig. 5D), they resemble clay-clast aggregates, which form in experimental and natural fault gouges deformed at seismic slip rates under undrained conditions (Boutareaud et al., 2008), but also at subseismic rates in other experiments (Han and Hirose, 2012). Cataclasite clasts are subrounded and contain early calcite veins (Figs. 5A and 5D), but no veins cut the matrix, which is instead cemented by disseminated carbonate (Fig. 5B). We infer a cyclical history of mineralization, shear, and fragmentation, but we suggest that once the clay-rich gouge formed, the material was not competent enough to experience fractures, into which late veins crosscutting the matrix fabric would have precipitated.

Disaggregated veins of similar gouge observed in adjacent cataclasite above the fault, and the fact that there are two discrete gouge layers in DFDP-1B, require that, through time, not all slip was localized within a single gouge layer. This delocalized behavior is to be expected since the gouge displays velocity-strengthening behavior at low temperatures and pressures (Boulton et al., 2012, 2014). Given these properties, it should be prone to aseismic creep. Nevertheless, paleoseismic investigations indicate that the fault zone accommodates coseismic slip (e.g., Berryman et al., 2012; Wells et al., 1999). Such seismic behavior is probably stimulated by ruptures initiating elsewhere within the fault zone (Faulkner et al., 2011; Noda and Lapusta, 2013; Boulton et al., 2014).

Unit 6: Lower Cataclasites

Lower cataclasites locally preserve gneissic fabrics within clasts (Figs. 5G and 6); these fabrics likely developed during ductile shear accommodated by crystal plasticity (Sibson, 1977). We cannot say whether this was in the modern Alpine fault footwall, or during some earlier deformation event such as that which yielded the Fraser complex (Rattenbury, 1991) or Cretaceous shearing (Klepeis et al., 1999). There is a pervasive brittle overprint; fractured but not rotated clasts (e.g., Figs. 5E and 5G) indicate grain size reduction sometimes occurred by comminution (Sammis et al., 1986), while calcite veins (Fig. 5E) suggest that hydrofracturing also played a role in grain-size reduction. More pervasive hydrous alteration of feldspars to sericite and saussurite in fractured zones records transient passage of fluid through the rock. Elsewhere, the fragmented clasts have been rotated and mixed during progressive shear (e.g., Fig. 5G). As in units 3 and 5, textures indicate that multiple cycles of brecciation and cementation occurred in the generation of these rocks (e.g., Fig. 5E). Local zones of cataclasite are observed at both thin-section (Fig. 5G) and core scales (Figs. A2P and A2Q). Furthermore, there is no systematic concentration of more or less comminuted material throughout the core recovered from this unit.

Unit 7: Breccias

The angular, uncemented clasts that make up unit 7 were probably generated by comminution. The uncemented nature of the breccia means a matrix was not preserved during thin-sectioning, so we cannot presently tell whether fragmentation was tectonic, drilling-induced, or both. Within the breccia clasts, the spaced foliation of fairly fine-grained (20–50 μm) quartz and feldspar/muscovite domains (Fig. 5H) shows an interconnected weak layer morphology (Handy, 1990). Quartz grain elongation is prominent, and we infer that quartz layers experienced continuous creep accommodated by crystal plasticity. However, there is no evidence of crystal plasticity in feldspar (e.g., recrystallization, undulose extinction, or strain twins), so the temperatures under which this deformation occurred are broadly constrained to 300–450 °C (Tullis, 2002).

DISCUSSION OF INFERRED PROTOLITHS

Identification of fault rock protoliths is key to constraining fault zone architecture, including assessing if there has been local imbrication of footwall (Australian plate derived) slices into the hanging wall. Toy (2008) presented a discussion of how we might differentiate the protoliths of the various Alpine fault zone lithologies, concluding that bulk-rock major- or minor-element chemistry signatures are not necessarily diagnostic of different protoliths and that the presence or absence of certain minerals is the most useful diagnostic indicator of protolith in these rocks. Pacific plate rocks are derived from monotonous sequences of quartzofeldspathic metapsammite and interbedded pelite of the Rakaia terrane, together with minor chert and mafic volcanic rocks. The Alpine Schist mylonites derived from the metasediments commonly contain oligoclase feldspar and garnet, whereas those from the mafic rocks (now amphibolites) contain hornblende ± garnet (Grapes and Watanabe, 1992). Mylonites and cataclasites derived from an Australian plate protolith include both granitoids and Greenland Group quartzose metasediments (Nathan, 1976; Tulloch, 1988). From these rocks, one expects orthoclase feldspar and/or albite, and also allanite.

We observe that most rocks above the principal slip zone in outcrop contain abundant oligoclase and hornblende, and therefore identify them as having a Pacific plate protolith, including likely elements of both the Rakaia terrane (MacKinnon, 1983; Mortimer, 2004; Sutherland et al., 2011) and the Aspiring lithologic association (Craw, 1984; Norris and Craw, 1987). However, modally abundant allanite indicates that some mylonites and banded ultramylonites are derived from the Australian plate. Poor outcrop exposure obscures the contact between Australian plate–derived rocks and more typical hanging-wall mylonites.

Unit 1 gray and dark-green ultramylonites are similar macro- and microscopically to the general description of ultramylonite provided by Toy et al. (2008, 2010), containing oligoclase, biotite, and hornblende, and they are likely derived from hanging-wall (Pacific plate) protoliths. Unit 2 brown-green-black ultramylonites differ from unit 1 in containing a disjunctive cleavage and a mineral assemblage including epidote, chlorite, and albite. These fabrics and mineral assemblages are consistent with formation of a retrograde mineral assemblage during progressive exhumation. Feldspar porphyroclasts present in unit 2 are consistent with derivation from footwall granitic rocks; however, much of unit 2 does not contain such porphyroclasts and appears macroscopically similar to other ultramylonites for which a hanging-wall protolith is most likely.

Units 3 and 4 are versions of units 1 and 2 that have undergone variable cataclasis and so may also have both hanging-wall and footwall protoliths. A progressive change in unit 3 and 4 fault rock coloration near the principal slip zone could indicate either a different protolith or differences in the way in which or the extent to which the rock has been altered during fluid-rock interactions. The latter interpretation is preferred since permeability, which is affected by the presence of alteration minerals (phyllosilicates and fracture-sealing carbonates), also progressively reduces through this zone (Sutherland et al., 2012; Carpenter et al., 2014).

A footwall origin was inferred by Townend et al. (2013) for unit 6 material immediately below PSZ-1 in DFDP-1B, based on the presence of orthoclase and on its petrophysical properties (especially high natural gamma radioactivity). Our observations of flame perthite, which results from strain-enhanced exsolution of trace Na from K-feldspar (Fig. 6A; Pryer and Robin, 1995) and myrmekite, an intergrowth of quartz and anorthite, intimately associated with K-feldspar (Fig. 6B; Castle and Lindsley, 1993) confirm the original presence of orthoclase. Furthermore, gneissic to granitic textures apparent in unit 6, particularly unit 6a (Fig. 6), are similar to textures described in footwall Fraser complex units by Rattenbury (1991) but not reported from any known hanging-wall lithology nearby.

DISCUSSION OF ALPINE FAULT ARCHITECTURE

We consider two end-member models for the way deformation is distributed in the brittle part of a major fault zone. Either (1) shear is very localized at shallower depths, where a principal slip zone develops, but at greater depth, the cataclastic displacement is within a broad shear zone, all of which accomplishes shear at a lower bulk strain rate than within the shallower localized zone (Fig. 7A); or (2) strain rate increases toward the center of the shear zone at all depths. In the latter case, "wider" parts of the exhumed fault rock developed by small increments of displacement on a variety of structures distributed around the fault core, throughout the entire depth of the seismogenic zone (Fig. 7B).

As illustrated in Figure 2C, cataclasites (units 3–6) comprise ~20%–40% of sampled rock throughout the core, and >50% in the 20 m of rock immediately surrounding all principal slip zones. This analysis does not suggest a gradual intensification of the cataclastic fabric with proximity to the principal slip zone. However, the overall proportion of unit 4 foliated cataclasite increases toward the principal slip zone, as does the intensity of the phyllosilicate foliation within this unit, while the overall grain size decreases, indicating a gradual increase in total shear strain within the brittle part of the fault zone toward the principal slip zone.

We also recognize that principal slip zone gouges are distinct. They have mineralogy (notably smectites; Table 1) compatible with significant alteration at shallow depth (<150 °C; Inoue and Utada, 1991; Moore and Reynolds, 1997). Some of these minerals are authigenic (Schleicher et al., 2015). Principal slip zone gouges have accommodated significant shear

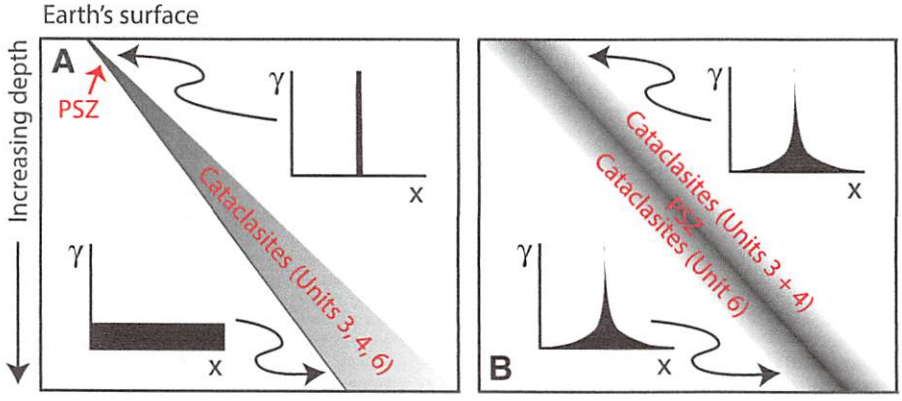

Figure 7. Schematic models of the spatial distribution of strain within a crustal fault zone. Gray shade indicates strain, γ, (or strain rate) at that position (where *x* is horizontal position) within the system. (A) Model 1: strain is distributed into a progressively widening zone with increasing depth. (B) Model 2: strain is focused in the fault zone center throughout deformation, and minor structures accommodate smaller increments of off–principal slip zone damage at all depths. The graphs illustrate the distribution of strain across the zone at depth within the brittle regime, and at the surface in each model. Red text labels indicate regions of generation of principal slip zone (PSZ; unit 5 gouge) and the cataclasites observed in the core for each of these models.

displacement in multiple increments of slip, some demonstrably coseismic (producing pseudotachylyte). Centimeter-scale layering of different grain sizes (Fig. 4N) and mineralogy is characteristic. Given that grain-size reduction in these materials likely results from and is proportional to strain (Blenkinsop, 1991), the presence of these grain-size variations indicates that strain is not uniformly distributed through the entire gouge layer. It is possible that a protracted history of localized deformation within the deeper parts of the fault zone has been overwritten in these materials by multiple increments of slip at shallow levels.

The cataclastic rocks and gouges described in the DFDP-1 core (units 3–6) have demonstrably accommodated some shear displacement, a process which generated fragments by comminution that were subsequently reduced in size by abrasion during ongoing shear. In the overlying unit 1 and 2 ultramylonites, most brittle structures are low-displacement fractures (Fig. A2), which are variably decorated by clay minerals but not necessarily cemented. Unit 7 breccia also seems to have experienced in situ fragmentation without significant shear, which would be manifest as rotation and displacement of fragments with respect to one another. In a model where a fault core has accommodated a large shear strain, while the damage zone contains fault-related structures but did not accommodate significant shear (Chester and Logan, 1986; Caine et al., 1996), units 3–6 comprise the fault core of this plate-boundary structure, and units 1, 2, and 7 represent the surrounding damage zone.

We cannot presently say how far the damage zone extends from the principal slip zone, as the fractures that typify it are present throughout the sampled core. Damage zones with thicknesses of 30–2000 m have been described around other mature strike-slip structures (e.g., Fialko et al., 2002; Mitchell and Faulkner, 2009; Lin and Yamashita, 2013), suggesting we sampled only part of the Alpine fault damage zone in this study. Townend et al. (2013) observed that fractures large enough to be observed by acoustic televiewer decreased in density toward DFDP-1B PSZ-1 in the hanging wall. This observation seems to contradict the typical increase in fracture density toward the principal slip zone described elsewhere (e.g., Mitchell and Faulkner, 2012; Johri et al., 2014). Townend et al. (2013) interpreted the observed changes in fracture density and seismic velocity near the principal slip zone to reflect interaction between fracture-creating and fracture-sealing processes during the seismic cycle. However, it might alternatively suggest that the open fractures are related to stress relief and are a function of shallow depth rather than proximity to the fault.

Sutherland et al. (2012) also commented on the relationships among a principal slip zone (unit 5), the fault core (units 3, 4, 6), and damage zone (units 1, 2, 7), and further highlighted that there is a distinct "alteration zone" that overprints the fault core and part of the damage zone. As the figures in this paper reveal, cementation and alteration by passage of fluids occurred episodically throughout the evolution of the fault zone materials. We hypothesize that the sequential activation of multiple structures accommodating shear displacement within the cataclastic zone (model 2, Fig. 7B) contributed to damage formation, coseismic and aseismic strain accommodation, and fluid migration within this alteration zone. In order to understand this relationship, future studies need to constrain pressure and temperature from mineral assemblages associated with each of the different styles of structures, and focus on petrogenetic sequences. Such studies would also enable strain profiles spanning the fault zone to be constructed for a variety of depths, which is needed if we are to differentiate fully which of the models suggested in Figure 7 is most realistic.

CONCLUSIONS

The cores retrieved during DFDP-1 provide the first continuous transect from the hanging wall to the footwall of the Alpine fault at a single location and thus offer a rare opportunity to define and interpret fault rocks with known spatial relationships. From detailed descriptions of the fault rocks, we draw the following conclusions:

(1) The distribution of lithologies in the sampled core is not simple or monotonic; in particular, the cataclastic rocks comprise material that may have been derived from both the Australian and the Pacific plates, which is only possible if the zone of focused brittle shear moves laterally over time, or includes multiple strands at greater depths.

(2) Based on the types of brittle structures observed, we can differentiate the lithological units sampled into a distinct principal slip zone (unit 5), fault core (units 3, 4, 6), and damage zone (units 1, 2, 7). The principal slip zone and fault core are extremely localized, with total thicknesses of <<1 m and <20–30 m, respectively. The damage zone has a minimum thickness of 70 m (the distance it extends above the principal slip zone). DFDP-1 did not enable the distribution of damage below the principal slip zone to be determined.

(3) The nature and intensity of cataclastic fabrics are spatially highly variable. Notably, there is evidence of localization within the principal slip zone and within the fault core, and the foliation in the fault core intensifies toward the principal slip zone, indicating more total strain was accommodated there. We present two contrasting models for distribution of strain with depth in the brittle regime consistent with these observations: (1) localization increasing upwards within the brittle crust; or (2) localization being similar throughout the brittle crust. Validation of either model requires more detailed study of the relationships between mineralogy and structures, so that strain profiles across the fault zone at a variety of pseudodepths can be constructed.

APPENDIX 1: DESCRIPTIONS OF TYPICAL ALPINE FAULT ZONE ROCKS IN OUTCROP

Descriptions are based on oriented samples of representative rock types from which oriented polished thin sections were made and examined using standard petrographic and electron-microscopic techniques.

Fault rock nomenclature broadly follows the scheme recently summarized by Woodcock and Mort (2008). These descriptions are grouped according to whether they are derived from hanging wall or footwall; evidence for this interpretation is discussed in the section entitled "Discussion of Inferred Protoliths."

Hanging Wall–Derived Mylonite Series

Alpine Schist–Derived Mylonites

Previous workers, in particular Norris and Cooper (2007) and Toy et al. (2012), have differentiated "Alpine Schist–derived mylonites," which are the most common constituent of the Alpine fault hanging wall that can be found in stream outcrops, into three structural groups. (1) Ultramylonites with S (i.e., surface)–dominated fabrics (in the sense of Flinn, 1965) but indistinct continuous foliations (in the sense of Piazolo and Passchier, 2002) have accommodated significant simple shear strains ($\gamma \sim 150$; Toy et al., 2013) and crop out in the ~100 m immediately overlying the fault principal slip zone; (2) mylonites with S-dominated fabrics of millimeter-spaced quartz-feldspar and mica ± amphibole layers have accommodated intermediate simple shear strains ($\gamma \sim 110$; Toy et al., 2013) and crop out 100–300 m structurally above the principal slip zone; and (3) protomylonites, with L-S fabrics, also have millimeter- to centimeter-spaced foliations of quartz-feldspar and mica ± amphibole, but these may retain isoclinal fold hinges (formed during deformation of the precursor Alpine Schist; Little et al., 2002a) and are distinctly transected by millimeter- to centimeter-spaced extensional shear bands with synthetic sense to the Alpine fault. Protomylonites have accommodated much lower bulk simple shear strains ($\gamma \sim 11.5$; Toy et al., 2013) and crop out ~300–1000 m structurally above the principal slip zone. Beyond these mylonites, the protolith is an L-S tectonite commonly described as the "Alpine Schist," with a centimeter- to decimeter-spaced foliation of quartz-feldspar and mica layers, and distinct quartz rod lineations plunging approximately downdip, rarely containing both synthetic and antithetic shear bands (Little et al., 2002a, 2002b). These three lithologies are illustrated in Figure 2 of Toy et al. (2012).

At Gaunt Creek, these mylonite-series rocks are mostly (96% of outcrop; Toy, 2008) medium gray, reflecting an average quartzofeldspathic mineralogy of 40%–50% quartz, 11%–24% oligoclase feldspar, 14%–33% biotite (which may be partially replaced by chlorite), <16% muscovite, and 2%–5% garnet + calcite + accessories, such as rutile, ilmenite, and apatite. Less than 4% of outcropping mylonite-series rocks are of metabasic composition (Fig. 7a *in* Toy et al., 2010), with bottle to minty green color, comprising 30%–50% hornblende, 15%–30% biotite (which is commonly partially replaced by chlorite), 20% each of quartz and oligoclase feldspar, and <10% calcite + epidote + accessories. Metabasite layer

thicknesses range from 5 cm to 2 m in thickness, and, within them, tectonite fabrics are heterogeneously developed; some layers have planar to shear-band–transected spaced foliations as in surrounding quartzofeldspathic mylonite, while others are virtually devoid of mineral preferred alignments. Other distinctive, but volumetrically insignificant outcropping lithologies are centimeter- to meter-thick metacherts, which are pink-orange in color and contain 50%–90% quartz, 5%–40% garnet, and <10% muscovite + biotite + accessories; and pegmatites (Fig. 4 *in* Norris and Cooper, 2007) of decimeter-scale or narrower widths that have similar bulk mineralogy to quartzofeldspathic mylonite-series rocks, but are coarser-grained so that books of muscovite <1 cm and K-feldspar and plagioclase porphyroclasts <0.5 cm can be differentiated by the naked eye.

Toy (2008) and Toy et al. (2008) noted distinctive microstructural characteristics within the mylonite series. Among these, quartz aggregates commonly contain large (<4 mm in protomylonites; 1 mm in mylonites) elongate grains (axial ratios 1:3–1:10) that display undulose extinction, subgrains, and coarsely interlobate grain boundaries. A separate, microstructurally distinct population of grains makes up less than 50% of grains in protomylonites, 50%–90% of grains in mylonites, and >90% of grains in ultramylonites. These grains are smaller (average 30 µm; of comparable size to subgrains), are less elongate (axial ratios ~1:2), have less marked undulose extinction, have coarsely interlobate or straight to gently curved grain boundaries, and have triple junctions generally subtending 90°–90°–180° angles. Plagioclase feldspars may have weak undulose extinction, but they lack deformation twins or subgrains, and they do not display core-mantle textures; in other words, they are porphyroclastic. Larger micas (<2 mm in length) may contain spiraled inclusion trails of graphite and are warped but usually not kinked. They are surrounded by or contain zones of smaller (<200 µm), more equant grains parallel to their basal plane. Large biotites (of order of 1 mm in length) are usually brown (high Fe:Ti); smaller biotites (<100 µm) are generally green (low Fe:Ti). Hornblendes may have weak undulose extinction but mostly appear to have acted as porphyroclasts, although they may have rotated into coincidence with foliation. Calcite may be interstitial to quartz or hornblende grains, in which case it is fine-grained (<10 µm), or it may occur as larger (submillimeter) grains in veins, in which case these grains mostly contain narrow, closely spaced e-twins (type I twins of Ferrill et al., 2004).

Typical structures overprinting these mylonite-series rocks include quartz veins at a variety of angles (including parallel) to foliation, ranging up to a meter in length and 20 cm in width, but mostly less than 10 cm long and 1 cm wide. Some of these veins are folded (Fig. 2 *in* Toy et al., 2010). They display a variety of microstructures, ranging from those similar to observed quartz in the host mylonite through to aggregates of sub-millimeter-sized, equant grains with patchy undulose extinction and very finely interlobate grain boundaries. There are also quartz + carbonate veins, best described by Toy et al. (2010) and Menzies et al. (2014); these are usually oriented at high angles to foliation or infill the necks of "foliation boudinage" structures, and are particularly prevalent in metabasites (Fig. 7 *in* Toy et al., 2010). They contain fluid inclusions indicating vein precipitation at ~325 °C and ~40 MPa, compatible with a depth exceeding 8 km, assuming hydrostatic conditions in a Si + Ca–bearing fluid (Toy et al., 2010). Oxygen and hydrogen stable isotope compositions indicate the fluids from which they precipitated are meteoric in origin (Menzies et al., 2014). Late fractures that transect the mylonitic foliation at moderate or high angles may have millimeter-thick quartz + chlorite infills, and there is commonly a distinct pale-green halo, a centimeter or less in thickness, around these structures. Shear sense on moderately dipping fractures is generally sinistral-reverse; steeply dipping fractures do not show shear offset.

Locally, millimeter-thick pseudotachylyte and ultracataclasite veins (Figs. 3 and 4 *in* Toy et al., 2011), and zones of fragmented and slightly chloritized mylonite, <30 cm thick, parallel the foliation; in places within these fragmented zones, there are more distinct clayey gouges, <1 cm in thickness, again parallel to foliation. Late brittle faults, a few with clay gouges hosting subrounded fragments of mylonite <1 cm in diameter may also crosscut the mylonitic foliation at moderate to high angles. Striae within these structures generally indicate strike-slip or normal kinematics, suggesting they accommodate near-surface adjustments of the overthrust fault rock, rather than solely reflecting the oblique-dextral reverse shear imposed on the Alpine fault by far-field plate motions.

Finally, almost all mylonites are transected by joints with subdecimeter spacings. These have not yet been subject to systematic study, and it is not known if orientations, densities, or spacings change systematically across the zone.

Green-Brown and Dark-Gray Planar Foliated Ultramylonites (Figs. A1C and A1F)

This ultramylonite lithology has a field appearance that is distinct from the "Alpine Schist–derived ultramylonites." These "green-brown and dark gray planar foliated ultramylonites" (Toy et al., 2008) are only common in the ~50 m or so of outcrop immediately above the principal slip zone at Gaunt Creek, near the DFDP-1 boreholes; they also outcrop over comparable thickness farther south at Stoney Creek and Waikukupa River (Fig. 1). However, few other surface outcrops expose the material immediately above the principal slip zone, so their true distribution is difficult to assess.

They have either a millimeter-spaced cleavage defined by intercalated quartz-rich and quartz-poor horizons, or a more continuous foliation that is revealed in thin section to be defined by submillimeter-thickness seams of optically unidentifiable minerals, which we infer are particularly resistive to dissolution, probably representing solution seams. The unit is generally fractured but not to the extent that it could be classified as a protocataclasite; that is, it does not have a significant amount of "matrix," which we define here as fine-grained particulate material generated by comminution during brittle shearing or by alteration/reaction. Wedge-shaped fragments of differently colored, foliated rock, possibly reflecting compositional variations within the protolith, are found in fault contact within this unit. These fault contacts are both parallel and oblique to foliation and are commonly decorated by glassy blue pseudotachylyte (Toy et al., 2012).

Hanging Wall–Derived Cataclasite Series

Toy (2008) identified that cataclasites (sensu stricto) exposed in the Alpine fault hanging wall are mint green, containing patchily distributed cream-colored lozenges (early veins) and blue-gray layers or veins (altered pseudotachylyte or very fine-grained gouge; Fig. 9 *in* Toy et al., 2011). In outcrop at Gaunt Creek, there is gradation to a more olive-green color over ~30 m into the hanging wall, perpendicular to the fault plane. The cataclasites are mostly unfoliated, but rare continuous to millimeter-spaced white-cream banded foliation is locally observed; this is probably a remnant texture from the protolith Alpine Schist.

The predominant mineralogy is quartz-feldspar-biotite-muscovite-accessories ± hornblende, calcite, garnet. Chlorite after biotite and actinolite after hornblende are more common than in the protoliths, as are neomineralized calcite, quartz, and disseminated pyrite (Toy et al., 2011).

Thin-section-scale observation reveals abundant subrounded to angular plagioclase feldspar porphyroclasts altered to fine clay minerals and internally microfractured along cleavage planes. These porphyroclasts are bounded by and are sometimes offset by shear on a network of dark hairline surfaces that commonly continue into patches of more angular, finer-grained material or thicker lozenges of titanite + opaques + clay minerals. These surfaces define an anastomosing foliation that could also be called a disjunctive cleavage. Interstitial large quartz and finer (<100 µm) untwinned polycrystalline quartz and calcite are common. In places, these neocrystallized aggregates completely support/surround porphyroclasts.

Overprinting structures include the aforementioned blue-gray pseudotachylytes or fine-grained gouges displaying fault vein and injection vein habits (cf. Sibson and Toy, 2006), as well as medium-brown to reddish brown, rarely vesicular patches of pseudotachylyte up to 5 cm in width (see also Fig. 10 *in* Toy et al., 2011). These are crosscut by millimeter- to centimeter-thick faults containing uncemented cataclasite to ultracataclasite. The latest-generation structures are sub-decimeter-thick zones of incohesive fault breccia comprising uncemented angular clasts ranging from clay to pebble size. There are no published summaries of systematic orientation relationships for these features.

Principal Slip Zone Gouges

Boulton et al. (2012) presented detailed descriptions and illustrations (their Figs. 2 and 3) of these materials. In summary, the gouges are commonly distributed in sharply (but sometimes undulatory) bounded layers defined by variations in matrix color (generally gray-brown to blue-gray), or clast proportion or composition. Layers range up to 50 cm thickness but are usually only a few centimeters. They may be uncemented to cemented by cryptocrystalline calcite or amorphous iron oxide (limonite or goethite) in surface outcrops. The most coherent samples probably achieve that state due to subaerial drying; they become incohesive again when wetted.

Clasts, which are generally subangular and <1 mm in diameter, comprise <40% of the rock. They include single mineral grains of quartz, feldspar, carbonate, opaques, and phyllosilicate as well as fragments of metamorphic quartz, vein quartz, reworked gouge, and vesicular pseudotachylyte, and they are supported by matrices of clay-sized particles. In outcrop, fabric is defined by alignment of long axes of clasts oblique to layer boundaries. In thin section, a similarly inclined fabric is rarely defined by aligned phyllosilicates (chlorite, illite-muscovite).

No mesoscale or macroscale structures crosscut the principal slip zone gouges systematically. However, we have observed high-aspect-ratio (greater than 1:20) veins of gouge branching away from the main layering and crosscutting earlier-formed gouge layers (Toy and Mitchell, 2014).

Footwall-Derived Mylonite Series

These lithologies are most commonly exhumed in the immediate hanging wall and footwall, and so they rarely crop out. However, DFDP-1 boreholes sampled this part of the sequence. These lithologies probably comprise part of the "green mylonites" noted by Sibson et al. (1979, 1981), but there are few detailed descriptions in the peer-reviewed literature. Thus, representative hand and thin section photomicrographs derived from Toy (2008) are presented (Fig. A1), and these rocks are described in detail here.

Augen ultramylonites and banded ultramylonites (Figs. A1A–A1D) make up <50% of outcropping mylonite sequence at Waitaha River and Harold Creek (Fig. 1) but become less predominant further south; at an unnamed tributary to the north of Little Man River (Fig. 1), they have a maximum thickness of ~20 m. The most southerly outcrops known are at Gaunt Creek, near the DFDP-1 site, where they are encountered in a thin wedge <10 m in thickness. Mapped geometry suggests that these units are bounded by faults oblique to foliation, but in most outcrops, the contacts with surrounding "Alpine Schist–derived mylonites" are obscured (Toy, 2008). At Harold Creek, one contact does crop out, and here it is a near-vertical, approximately E-W–striking zone of yellow-brown clay gouge containing ~50% subrounded mylonite clasts.

Augen ultramylonites are brown, brown-gray, locally bottle green, or cream, with modally abundant hornblende, and they are nonfoliated to weakly foliated, with foliation defined by micaceous and quartz-rich layers with pinch-and-swell structure. A very fine-grained (5–30 µm) matrix of quartz + phyllosilicates (chlorite, sericite?) hosts <20% augen of <5 mm length composed of sericitized and microfractured plagioclases (mostly albite) with interstitial calcite. Sigmoidal clasts are not usually visible in hand specimen but are apparent in thin section. Augen of allanite with clinozoisite rims and diameters of 50–500 µm are relatively abundant (>5%).

Banded ultramylonites (Figs. A1B and A1E) crop out in association with augen mylonites and may be intercalated on the meter scale. They have a planar foliation visible as medium-

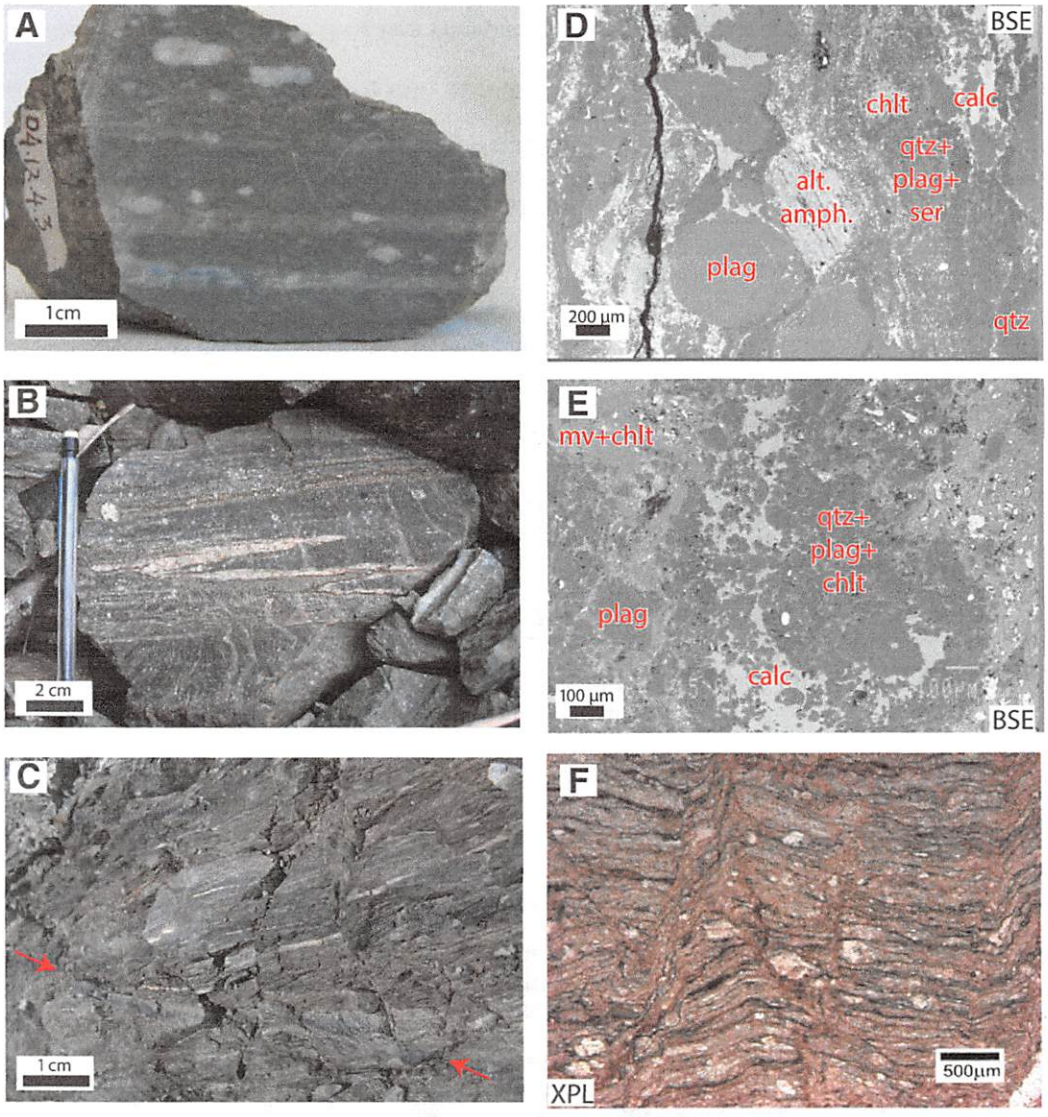

Figure A1. Photomicrographs and photographs illustrating distinctive mylonitic lithologies not previously described that have correlatives in Deep Fault Drilling Project (DFDP-1) core. Abbreviations for mineral labels follow Whitney and Evans (2010); additionally, alt amph—altered amphibole, XPL—cross-polarized light, BSE—backscattered electron. "OU" sample numbers relate to the University of Otago Geology Department collection's curation system. (A) OU77718: Hand specimen of augen ultramylonite, Harold Creek. (B) Typical outcrop photograph of transitional augen ultramylonite–banded ultramylonite, Harold Creek. Isoclinal folds of pale (feldspar-rich) layers are typical of the latter unit. (C) Green-brown and dark-gray planar foliated ultramylonites in outcrop, Gaunt Creek. Note the fault (between arrows) decorated by darker material than the matrix; this may be ultracataclasite or pseudotachylyte. (D) OU77710: Harold Creek. Typical augen ultramylonite. Feldspar porphyroclasts with pressure shadows composed of calcite and quartz are embedded in a fine matrix of quartz and phyllosilicates. (E) OU77718: Harold Creek. Typical banded ultramylonite. (F) OU77827: Gaunt Creek. Typical green-brown and dark-gray planar foliated ultramylonite. Bands of concentrated opaques tracing subhorizontally across the image are inferred to be solution seams. These are offset by high-angle conjugate microshears.

green-gray and light-gray-white bands that are 1–3 mm thick. This foliation is locally folded into decimeter-scale, tight to isoclinal structures with rounded hinges and thickening of layering into the hinges. They rarely contain small (<1 mm) plagioclase augen. Microstructurally, they are either similar to augen ultramylonites, or they comprise aggregates of subrounded and equant quartz and plagioclase grains or masses of <50-µm-long muscovite and chlorite with a wide variety of grain orientations, cemented by <50% calcite.

The most common overprinting structures in this rock type are pseudotachylytes and veins. Pseudotachylytes occur as both centimeter-thick, foliation-parallel veins and as chaotic networks and injected masses up to tens of centimeters across. These veins are commonly zoned and flow banded (cf. Bossière, 1991) and may be partially or completely replaced by chlorite (Toy et al., 2011).

Millimeter-thick adularia, quartz, and calcite veins crosscut the foliation at high angles, but many have been locally sheared into parallelism with the foliation. In thin section, we observed the same composition veins on much smaller scale (tens of micrometers in thickness) within plagioclase porphyroclasts, but truncated by wrapping foliations.

APPENDIX 2: DRILLING PROCEDURES AND CORE CURATION

All depths reported in this manuscript are "core depths." A +0.2 m correction should be applied to correlate with depths of wireline log data reported by Townend et al. (2013).

Coring was undertaken by advancing the bit in increments of <3.0 m (one "run"). The recovered core was split into sections <1.0 m in length. Sample or observation locations within the recovered material are denoted by "Hole.Run Number_Section Number.Depth below top of section (cm)," where Section Number = CC denotes the core catcher. The core was not oriented, and we do not know the relative orientation of most contiguous core sections, as they were rotated with respect to one another during acquisition. Up to 20 cm sections of core were usually destroyed on extraction from the core catcher, further complicating the matching between runs. Additionally, core was only recovered from ~50% of the drilled intervals due to difficult drilling conditions in the fractured rock.

Preliminary lithological and structural descriptions were undertaken on site, after which the core was sealed in plastic wrap and transported to more permanent storage facilities at the University of Otago, Dunedin. There, more comprehensive descriptions focusing on structures were undertaken, and core images were obtained from three different angles; these were stitched together in photographic software to give "unrolled core scan" images), and physical properties of the core (P-wave velocities, gamma-density, diameter, imaging) were measured using a Geotek multisensor core logger (MSCL). Finally, computed tomography (CT) scans of all core sections were obtained with medical-grade equipment in the Oncology Department of Dunedin Hospital. Following this, subsamples were separated from the core and distributed to collaborators.

APPENDIX 3: CHARACTERISTIC STRUCTURES

Certain types of structures (e.g., cataclasite zones, veins) were typically observed in each of the lithological units we define herein. These are demonstrated in the 180° core scan images, and examples of typical structures are presented here (Table A1). More thorough documentation of these structures will be presented in a later contribution.

ACKNOWLEDGMENTS

We thank Brent Pooley for making excellent thin sections of fragile fault rocks; Alex Pyne, Greg de Pascale, Jennifer Eccles, Mike Hasting, Jeremy Cole-Baker, Rob Langridge, Zoe Reid Lindroos, Bettina Fleming, and Richard Wing for enthusiastic help at the DFDP-1 site; and Hori-

TABLE A1. TYPICAL STRUCTURES IN FAULT ROCK LITHOLOGIES PRESENT IN DEEP FAULT DRILLING PROJECT (DFDP-1) CORES

Unit number and name	Typical structures
1. Gray and dark green ultramylonites	• Clay or cataclasite-filled fractures, <5 mm thick, containing clast-supported protocataclasite with angular, millimeter- to centimeter-diameter clasts. • Conjugate, open, unfilled fracture sets (Fig. 5A). • Approximately foliation-parallel microfaults containing one of: green-brown incohesive chloritic gouge, quartz-rich gouge (deformation-related gouge/alteration-related clay distinction unclear; Fig. A2B). • Millimeter-thick chlorite-epidote-quartz, just quartz, and possible calcite veins at high angle to foliation. • Rare "patchy" chloritic alteration. • Planar, foliation-oblique fractures commonly divide intact mylonite from fractured protolith to protocataclasite (i.e., unit 3b). • There is a gradual increase down core in the density of fractures (→ fractured protolith), and increase in density of zones of protocataclasite, commonly of 10 cm thickness. • Planar, foliation-parallel, flinty black to blue-black and sometimes glassy layers of millimeter thickness (pseudotachylytes and ultracataclasites; Fig. A2A). • Microscale shear bands (crenulations; Fig. A2C).
2. Brown-green-black ultramylonites	• Open fractures and millimeter-scale displacement microfaults at a variety of angles to foliation seem mostly drilling or handling-induced, but some are calcite-coated so must be primary; some are conjugate; all generally crosscut pseudotachylyte (Fig. A2D). • Millimeter-thick discontinuous white to orange quartz or calcite veins; commonly foliation-perpendicular (e.g., Fig. A2E). Orange color more prevalent in sections below run 45 in DFDP-1B. • Foliation-parallel but discontinuous white (probably quartz) veins up to a few millimeters in thickness, which may be deflected by the latest generation microfaults. • Rare salmon pink veins (e.g., Fig. A2E). • Boundaries between different constituent colors are commonly oblique to foliation and decorated by blue-gray, glassy material (altered ultracataclasite or pseudotachylyte; two instances are arrowed in Fig. A2D); less commonly by gouge (e.g., Fig. A2D). • These boundaries are also commonly offset on microfaults at high angles to primary contacts, with 5-cm-scale spacing or less (Fig. A2D). • Millimeter-thick flinty black layers parallel to foliation = pseudotachylyte?; may locally preserve fault and injection vein relationships; more common in black than brown ultramylonite. • Discrete faults; examples are described as "normal, associated with white veins, gouge-filled, <1.5 cm thick, filled with dark-brown ultracataclasite or with scaly fabric, anastomosing networks of brittle shear zones" (Toy et al., 2008). May form conjugate networks (e.g., Fig. A2F). • Some nonplanar quartz-rich segregations that may be bounded by bright blue material (also possibly pseudotachylyte), and crosscut by calcite veins (Fig. A2F). • Foliations within this material commonly have a range of dips, changing gradually through uniform-colored lithologies, or more abruptly on fault contacts.
3. Upper unfoliated cataclasites	• Microfaults of various orientations including foliation-parallel containing either green-brown incohesive chloritic gouge, quartz-rich gouge, or poorly sorted gouge with blue-gray clayey matrix (e.g., vertical fault in Fig. A2G). • Open fractures with quartz coating and millimeter-thick quartz veins (e.g., Fig. A2H). • Blue blebs (pseudotachylyte?) (arrowed in Fig. 5G, also similar to those in unit 4; as shown in Fig. A2J). • Boudinaged carbonate veins. • Faint pink veins of unknown composition. • Fragments of millimeter-thick calcite veins and less than centimeter-thick white or orange quartz or calcite (Fig. A2G). • Areas of cataclasite with different clast:matrix ratios and colors (range of browns and greens related to proportion of clay matrix) are commonly juxtaposed on a network of intersecting discrete faults at 40°–60° to the core axis (Figs. A2H and A2I). • Patches containing more coherent mylonitic foliation; commonly not rotated compared to adjacent fragments (Figs. A2G and A2I). • Boudinaged quartzofeldspathic lithology (e.g., Fig. A2G).
4. Upper foliated cataclasites	• Discontinuous, orange (?) quartz veins; documented orientations range from subvertical to parallel and perpendicular to lithological boundaries; commonly centimeters long and millimeters thick; also commonly brecciated. • Boudinaged/lensoidal quartzofeldspathic vein fragments <5 cm long (e.g., Fig. A2J). • Cataclastic fabric (shears) with Y-C orientations becoming more prevalent with depth (e.g., Fig. A2J). • Gouge-filled faults (e.g., between arrows, Fig. A2K). With increasing depth in the core, a network of intersecting structures of this type, typically dipping at 30° to the core axis become increasingly prevalent until by 1B.58_1 they are spaced at 5 cm or less. (Fig. A2K). • Blue-gray altered pseudotachylyte or fault gouge; layers (that may be discontinuous) parallel to foliation and as discontinuous blebs up to a centimeter think; generally disrupted by later discrete, millimeter-scale displacement brittle microfaults (between arrows and within dashed ellipse, Fig. A2I). • Remnants of green/black layering dissected by later high-angle faults (e.g., Fig. A2J).
5. Gouges	• Orange oxidized material (sulfides?) (arrowed in Fig. 6N). • Tensile crack network creating jigsaw blocks of gouge (Figs. 6M and 6R). • Open mechanical fractures (Figs. 6M, 6O, 6Q, and 6R). • Complex mingling of gouge colors is common—appearance is of injection veins sometimes offset by centimeter-scale displacement microfaults (Fig. A2M; arrowed in Fig. A2N). • Crosscutting injection veins of brown gouge (unit 5) originate from all principal slip zones (PSZs) and project into adjacent cataclasites (e.g., arrowed in Fig. A2O).
6. Lower cataclasites	
6a. White to white-gray granular cataclasite	• Abundant normal sense microshears millimeters wide and centimeters long containing much finer-grained white ultracataclasite in a network crosscutting the cataclasite (also observed in unit 6d). • Faint foliation suggested by color banding (e.g., Fig. A2P). • Black flinty layers crosscutting foliation (possible pseudotachylyte) (labeled pst? in Fig. A2Q).
6b. Dark-green foliated cataclasite	• Boudinaged lenses of quartz >15 cm long (Fig. A2P).
6c. Unfoliated gray to green clay-rich ultracataclasite to gouge	• Boudinaged lenses of quartz containing abundant fractures. Some of these are larger pods of material similar to unit 6a. • Sulfides (Fig. A2R). • Blue-gray pseudotachylyte or gouge blebs.
6d. Mixture of 6a–6c.	• Multiple light- to medium-gray, millimeter- to centimeter-thick gouges crosscut this material, many not parallel to the dominant foliation and some forming conjugate sets (e.g., Figs. A2Q and A2S). • Boudinaged lenses of quartz (Fig. A2P) and some larger (<3 cm thick and full thickness of core) pods of quartzose material (Fig. A2F; these are large pods of unit 6a). • Salmon pink to brown veins (Fig. A2T). • Gouge-filled fractures and shears. • In places the cataclastic foliation is folded at the <10 cm scale (so folds are visible in the core; e.g., Fig. A2U). • Blue-gray layers, and rarer black flinty layers mostly parallel to foliation (gouge or pseudotachylyte).
7. Breccias	• Fractures parallel to foliation (e.g., Fig. A2V). • Generally poorly preserved core (Fig. A2W). • Open fractures with calcite-epidote ± chlorite coating. • Cohesive fragments of core dissected by numerous gouges and composed of cataclasite fragments (Fig. A2X).

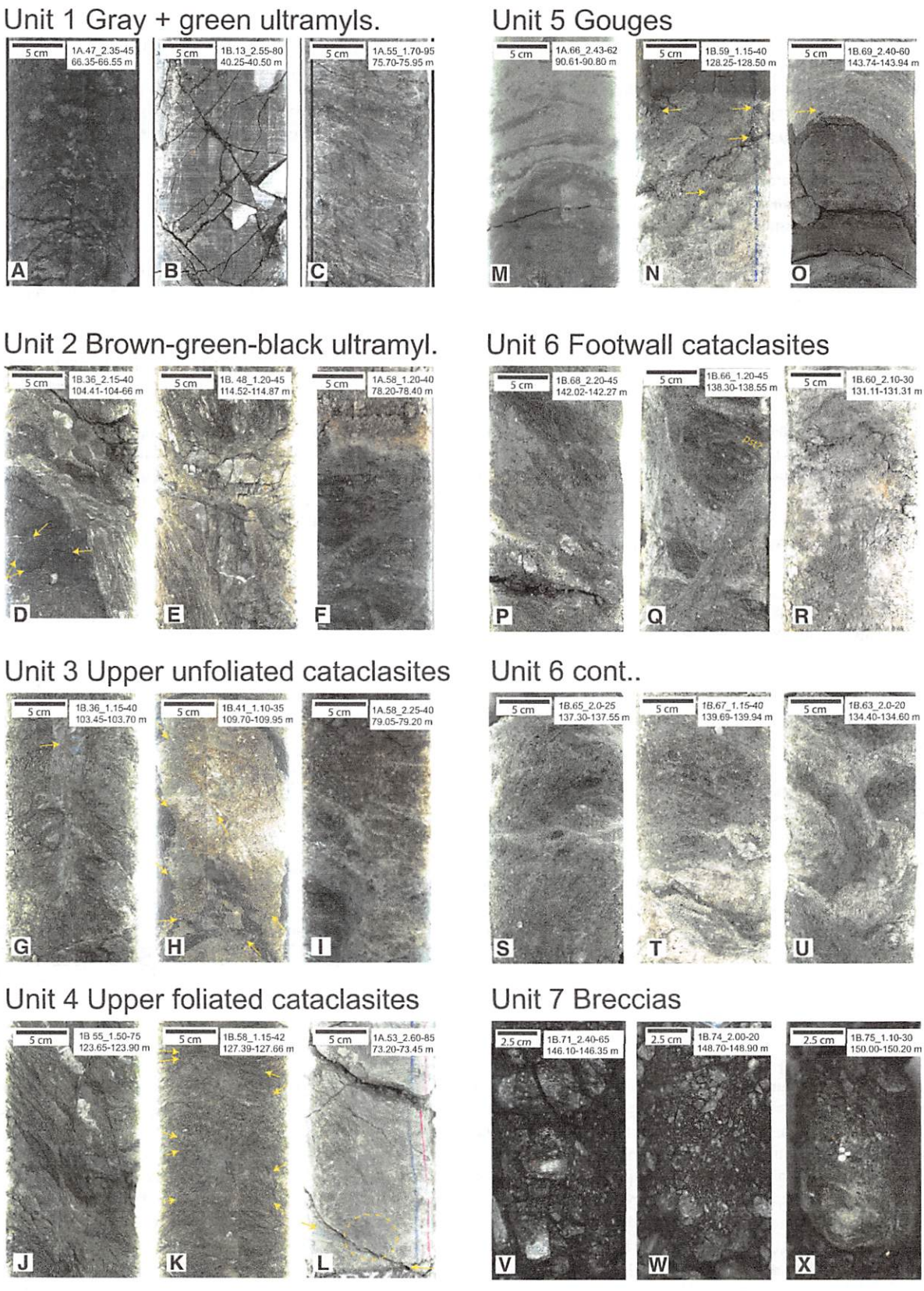

Figure A2. Unrolled 180° scans (5 cm scale bars) or flat scans (2.5 cm scale bars) of core sections illustrating typical structures in each of the lithological units. The various structures observed in each image are indicated in Table A1. Throughout, yellow arrows highlight microfaults. In Q, pst—pseudotachylyte.

zon Drilling, the Department of Conservation, White Heron Sanctuary Tours, and the Whataroa community for technical and logistical assistance during DFDP-1 drilling. DFDP-1 was funded by: GNS Science; Victoria University of Wellington; the University of Otago; the University of Auckland; the University of Canterbury; Deutsche Forschungsgemeinschaft and the University of Bremen; Natural Environment Research Council and the University of Liverpool; and the Marsden Fund of the Royal Society of New Zealand (NERC Grant Numbers NE/J024449/1, NE/G524160/1, NE/H012486/1). Discussion with Nick Mortimer and comments by Bob Holdsworth on early versions of this manuscript resulted in significant enhancements.

High-resolution images of all core sections and the full suite of core logs have been archived electronically and may be requested by contacting the first author. These scans are also presently archived by the International Continental Scientific Drilling Program (ICDP; http://alpine.icdp-online.org).

REFERENCES CITED

Beavan, J., Ellis, S., Wallace, L., and Denys, P., 2007, Kinematic constraints from GPS on oblique convergence of the Pacific and Australian plates, central South Island, New Zealand, *in* Okaya, D., Stern, T., and Davey, F., eds., A Continental Plate Boundary: Tectonics at South Island, New Zealand: American Geophysical Union Geophysical Monograph 175, p. 75–94.

Ben-Zion, Y., and Sammis, C.G., 2003, Characterization of fault zones: Pure and Applied Geophysics, v. 160, p. 677–715, doi:10.1007/PL00012554.

Berryman, K.R., Cochran, U.A., Clark, K.J., Biasi, G.P., Langridge, R.M., and Villamor, P., 2012, Major earthquakes occur regularly on an isolated plate boundary fault: Science, v. 336, p. 1690–1693, doi:10.1126/science.1218959.

Blenkinsop, T.G., 1991, Cataclasis and processes of particle size reduction: Paleogeophysics, v. 136, no. 1, p. 59–86.

Boese, C., Townend, J., Smith, E., and Stern, T., 2012, Microseismicity and stress in the vicinity of the Alpine fault, central Southern Alps, New Zealand: Journal of Geophysical Research, v. 117, no. B2, p. 1–20, doi:10.1029/2011JB008460.

Bossière, G., 1991, Petrology of pseudotachylytes from the Alpine fault of New Zealand: Tectonophysics, v. 196, p. 173–193, doi:10.1016/0040-1951(91)90295-4.

Boulton, C.J., 2013, Experimental Investigation of Gouges and Cataclasites, Alpine Fault, New Zealand [Ph.D. thesis]: Christchurch, University of Canterbury, 435 p.

Boulton, C., Carpenter, B.M., Toy, V.G., and Marone, C., 2012, Physical properties of surface outcrop cataclastic fault rocks, Alpine fault, New Zealand: Geochemistry Geophysics Geosystems, v. 13, no. 1, p. Q01018, doi:10.1029/2011GC003872.

Boulton, C., Moore, D., Lockner, D.A., Toy, V.G., Townend, J., and Sutherland, R., 2014, Frictional strength and stability of exhumed fault gouges in DFDP-1 cores, Alpine fault, New Zealand: Geophysical Research Letters, v. 41, p. 356–362, doi:10.1002/2013GL058236.

Boutareaud, S., Calugaru, D.-G., Han, R., Fabbri, O., Misoguchi, K., Tsutsumi, A., and Shimamoto, T., 2008, Clay-clast aggregates: A new structural evidence for seismic sliding?: Geophysical Research Letters, v. 35, p. L05302, doi:10.1029/2007GL032554.

Caine, J.S., Evans, J.P., and Forster, C.B., 1996, Fault zone architecture and permeability structure: Geology, v. 24, no. 11, p. 1025–1028, doi:10.1130/0091-7613(1996)024<1025:FZAAPS>2.3.CO;2.

Cande, S.C., and Stock, J.M., 2004, Pacific-Antarctic-Australia motion and the formation of the Macquarie plate: Geophysical Journal International, v. 157, p. 399–414, doi:10.1111/j.1365-246X.2004.02224.x.

Carpenter, B.M., Kitajima, H., Sutherland, R., Townend, J., Toy, V.G., and Saffer, D., 2014, Hydraulic and acoustic properties of the active Alpine fault, New Zealand: Laboratory measurements on DFDP-1 drill core: Earth and Planetary Science Letters, v. 390, p. 45–51, doi:10.1016/j.epsl.2013.12.023.

Castle, R.O., and Lindsley, D.H., 1993, An exsolution silica-pump model for the origin of myrmekite: Contributions to Mineralogy and Petrology, v. 115, no. 1, p. 58–65, doi:10.1007/BF00712978.

Chester, F.M., and Logan, J.M., 1986, Implications for the mechanical properties of brittle faults from observations of the Punchbowl fault zone, California: Pure and Applied Geophysics, v. 124, p. 79–106, doi:10.1007/BF00875720.

Cooper, A.F., and Norris, R.J., 1994, Anatomy, structural evolution, and slip rate of a plate-boundary thrust: The Alpine fault at Gaunt Creek, Westland, New Zealand: Geological Society of America Bulletin, v. 106, p. 627–633, doi:10.1130/0016-7606(1994)106<0627:ASEASR>2.3.CO;2.

Cowan, D.S., 1999, Do faults preserve a record of seismic slip? A field geologist's opinion: Journal of Structural Geology, v. 21, p. 995–1001, doi:10.1016/S0191-8141(99)00046-2.

Cox, S.C., and Barrell, D.J.A., 2007, Geology of the Aoraki Area: Lower Hutt, New Zealand, GNS Science, scale 1:250,000.

Cox, S.C., and Sutherland, R., 2007, Regional geological framework of South Island, New Zealand, and its significance for understanding the active plate boundary, *in* Okaya, D., Stern, T., and Davey, F., eds., A Continental Plate Boundary: Tectonics at South Island, New Zealand: American Geophysical Union Geophysical Monograph 175, p. 19–46.

Craw, D., 1984, Lithologic variations in Otago Schist, Mt. Aspiring area, northwest Otago, New Zealand: New Zealand Journal of Geology and Geophysics, v. 27, p. 151–166, doi:10.1080/00288306.1984.10422524.

Davey, F.J., Eberhart-Phillips, D., Kohler, M.D., Bannister, S., Caldwell, G., Henrys, S., Scherwath, M., Stern, T., and van Avendonk, H., 2007, Geophysical structure of the Southern Alps orogen, South Island, New Zealand, *in* Okaya, D., Stern, T., and Davey, F., eds., A Continental Plate Boundary: Tectonics at South Island, New Zealand: American Geophysical Union Geophysical Monograph 175, p. 47–72.

DeMets, C., Gordon, R.G., and Argus, D.F., 2010, Geologically current plate motions: Geophysical Journal International, v. 181, p. 1–80, doi:10.1111/j.1365-246X.2009.04491.x.

De Pascale, G.P., and Langridge, R.M., 2012, New on-fault evidence for a great earthquake in A.D. 1717, central Alpine fault, New Zealand: Geology, v. 40, p. 791–794, doi:10.1130/G33363.1.

Faulkner, D.R., Lewis, A.C., and Rutter, E.H., 2003, On the internal structure and mechanics of large strike-slip fault zones: Field observations of the Carboneras fault in southeastern Spain: Tectonophysics, v. 367, p. 235–251, doi:10.1016/S0040-1951(03)00134-3.

Faulkner, D.R., Mitchell, T.M., Rutter, E.H., and Cembrano, J., 2008, On the structure and mechanical properties of large strike-slip faults, *in* Wibberley, C.A.J., Kurz, W., Imber, J., Holdsworth, R.E., and Collettini, C., eds., Structure of Fault Zones: Implications for Mechanical and Fluid-Flow Properties: Geological Society of London Special Publication 299, p. 139–150.

Faulkner, D.R., Mitchell, T.M., Behnsen, J., Hirose, T., and Shimamoto, T., 2011, Stuck in the mud? Earthquake nucleation and propagation through accretionary forearcs: Geophysical Research Letters, v. 38, p. L18303, doi:10.1029/2011GL048552.

Ferrill, D.A., Morris, A.P., Evans, M.A., Burkhard, M., Groshong, R.H., and Onasch, C.M., 2004, Calcite twin morphology: A low-temperature deformation geothermometer: Journal of Structural Geology, v. 26, no. 8, p. 1521–1529, doi:10.1016/j.jsg.2003.11.028.

Fialko, Y., Sandwell, D., Agnew, D., Simons, M., Shearer, P., and Minster, B., 2002, Deformation on nearby faults induced by the 1999 Hector Mine earthquake: Science, v. 297, p. 1858–1862, doi:10.1126/science.1074671.

Flinn, D., 1965, On the symmetry principal and the deformation ellipsoid: Geological Magazine, v. 102, no. 1, p. 36–45, doi:10.1017/S0016756800053851.

Grapes, R., and Watanabe, T., 1992, Metamorphism and uplift of Alpine schist in the Franz Josef–Fox Glacier area of the Southern Alps, New Zealand: Journal of Metamorphic Geology, v. 10, p. 171–180, doi:10.1111/j.1525-1314.1992.tb00077.x.

Gratier, J., Richard, J., Renard, F., Mittempergher, S., Doan, M.L., DiToro, G., Hadizadeh, J., and Boullier, A.M., 2011, Aseismic sliding of active faults by pressure solution creep: Evidence from the San Andreas Fault Observatory at depth: Geology, v. 39, no. 12, p. 1131–1134, doi:10.1130/G32073.1.

Han, R., and Hirose, T., 2012, Clay-clast aggregates in fault gouge: An unequivocal indicator of seismic faulting at shallow depths?: Journal of Structural Geology, v. 43, p. 92–99, doi:10.1016/j.jsg.2012.07.008.

Handy, M.R., 1990, The solid-state flow of polymineralic rocks: Journal of Geophysical Research, v. 95, no. B6, p. 8647–8661, doi:10.1029/JB095iB06p08647.

Hirth, G., and Tullis, J., 1992, Dislocation creep regimes in quartz aggregates: Journal of Structural Geology, v. 14, p. 145–159, doi:10.1016/0191-8141(92)90053-Y.

Holdsworth, R.E., van Diggelen, E.W.E., Spiers, C.J., de Bresser, J.H.P., Walker, R.J., and Bowen, L., 2011, Fault rocks from the SAFOD core samples: Implications for weakening at shallow depths along the San Andreas fault, California: Journal of Structural Geology, v. 33, p. 132–144, doi:10.1016/j.jsg.2010.11.010.

Howarth, J.D., Fitzsimons, S.J., Norris, R.J., and Jacobsen, G.E., 2012, Lake sediments record cycles of sediment flux driven by large earthquakes on the Alpine fault, New Zealand: Geology, v. 40, p. 1091–1094, doi:10.1130/G33486.1.

Inoue, A., and Utada, M., 1991, Smectite-to-chlorite transformation in thermally metamorphosed volcanoclastic rock in the Kamikita area, northern Honshu, Japan: The American Mineralogist, v. 76, p. 628–640.

Johri, M., Dunham, E.M., Zoback, M.D., and Fang, Z., 2014, Predicting fault damage zones by modeling dynamic rupture propagation and comparison with field observations: Journal of Geophysical Research, v. 119, p. 1251–1272, doi:10.1002/2013JB010335.

Klepeis, K., Daczko, N., and Clarke, G., 1999, Kinematic vorticity and tectonic significance of superposed mylonites in a major lower crustal shear zone, northern Fiordland, New Zealand: Journal of Structural Geology, v. 21, p. 1385–1405, doi:10.1016/S0191-8141(99)00091-7.

Koons, P.O., 1987, Some thermal and mechanical consequences of rapid uplift; an example from the Southern Alps, New Zealand: Earth and Planetary Science Letters, v. 86, p. 307–319, doi:10.1016/0012-821X(87)90228-7.

Lin, A., and Yamashita, K., 2013, Spatial variations in damage zone width along strike-slip faults: An example from active faults in southwest Japan: Journal of Structural Geology, v. 57, p. 1–15, doi:10.1016/j.jsg.2013.10.006.

Little, T.A., Holcombe, R.J., and Ilg, B.R., 2002a, Ductile fabrics in the zone of active oblique convergence near the Alpine fault, New Zealand: Identifying the neotectonic overprint: Journal of Structural Geology, v. 24, no. 1, p. 193–217, doi:10.1016/S0191-8141(01)00059-1.

Little, T.A., Holcombe, R.J., and Ilg, B.R., 2002b, Kinematics of oblique collision and ramping inferred from microstructures and strain in middle crustal rocks, central Southern Alps, New Zealand: Journal of Structural Geology, v. 24, no. 1, p. 219–239, doi:10.1016/S0191-8141(01)00060-8.

Little, T.A., Cox, S., Vry, J.K., and Batt, G., 2005, Variations in exhumation level and uplift rate along the oblique-slip Alpine fault, central Southern Alps, New Zealand: Geological Society of America Bulletin, v. 117, p. 707–723, doi:10.1130/B25500.1.

MacKinnon, T.C., 1983, Origin of the Torlesse terrane and coeval rocks, South Island, New Zealand: Geological Society of America Bulletin, v. 94, p. 967–985, doi:10.1130/0016-7606(1983)94<967:OOTTTA>2.0.CO;2.

Mariani, E., Brodie, K., and Rutter, E., 2006, Experimental deformation of muscovite shear zones at high temperatures under hydrothermal conditions and the strength of phyllosilicate-bearing faults in nature: Journal of Structural Geology, v. 28, p. 1569–1587, doi:10.1016/j.jsg.2006.06.009.

Menzies, C.D., Teagle, D.A.H., Craw, D., Cox, S.C., Boyce, A.J., Barrie, C.D., and Roberts, S., 2014, Incursion of meteoric waters into the ductile regime in an active orogen: Earth and Planetary Science Letters, v. 399, p. 1–13, doi:10.1016/j.epsl.2014.04.046.

Mitchell, T., and Faulkner, D., 2009, The nature and origin of off-fault damage surrounding strike-slip fault zones with a wide range of displacements: A field study from the Atacama fault system, northern Chile: Journal of Structural Geology, v. 31, p. 802–816, doi:10.1016/j.jsg.2009.05.002.

Mitchell, T., and Faulkner, D., 2012, Towards quantifying the matrix permeability of fault damage zones in low porosity rocks: Earth and Planetary Science Letters, v. 339–340, no. C, p. 24–31, doi:10.1016/j.epsl.2012.05.014.

Moore, D.M., and Reynolds, R.C., 1997, X-Ray Diffraction and the Identification and Classification of Clay Minerals: Oxford, Oxford University Press, 375 p.

Mortimer, N., 2004, New Zealand's geological foundations: Gondwana Research, v. 7, p. 261–272, doi:10.1016/S1342-937X(05)70324-5.

Munsell, A.H., 1912, A pigment color system and notation: The American Journal of Psychology, v. 23, no. 2, p. 236–244, doi:10.2307/1412843.

Nathan, S., 1976, Geochemistry of the Greenland Group (Early Ordovician), New Zealand: New Zealand Journal of Geology and Geophysics, v. 19, p. 683–706, doi:10.1080/00288306.1976.10426314.

Niemeijer, A., and Spiers, C., 2005, Influence of phyllosilicates on fault strength in the brittle-ductile transition: Insights from rock analogue experiments, *in* Bruhn, D., and Burlini, L., eds., High-Strain Zones: Structure and Physical Properties: Geological Society of London Special Publication 245, p. 303–327, doi:10.1144/GSL.SP.2005.245.01.15.

Noda, H., and Lapusta, N., 2013, Stable creeping fault segments can become destructive as a result of dynamic weakening: Nature, v. 493, p. 518–521, doi:10.1038/nature11703.

Norris, R.J., and Cooper, A.F., 2001, Late Quaternary slip rates and slip partitioning on the Alpine fault, New Zealand: Journal of Structural Geology, v. 23, p. 507–520, doi:10.1016/S0191-8141(00)00122-X.

Norris, R.J., and Cooper, A.F., 2007, The Alpine fault, New Zealand: Surface geology and field relationships, *in* Okaya, D., Stern, T., and Davey, F., eds., A Continental Plate Boundary: Tectonics at South Island, New Zealand: American Geophysical Union Geophysical Monograph 175, p. 157–175.

Norris, R.J., and Craw, D., 1987, Aspiring terrane: An oceanic assemblage from New Zealand and its implications for terrane accretion in the southwest Pacific, *in* Leitch, E.C., and Scheibner, E., eds., Terrane Accretion and Orogenic Belts: American Geophysical Union Geodynamics Monograph 19, p. 169–177.

Norris, R.J., Koons, P.O., and Cooper, A.F., 1990, The obliquely-convergent plate boundary in the South Island of New Zealand; implications for ancient collision zones: Journal of Structural Geology, v. 12, p. 715–725, doi:10.1016/0191-8141(90)90084-C.

Okaya, D., Stern, T., Davey, F., Henrys, S., and Cox, S., 2007, Continent-continent collision at the Pacific/Indo-Australian plate boundary: Background, motivation, and principal results, *in* Okaya, D., Stern, T., and Davey, F., eds., A Continental Plate Boundary: Tectonics at South Island, New Zealand: American Geophysical Union Geophysical Monograph 175, p. 1–18.

Piazolo, S., and Passchier, C.W., 2002, Controls on lineation development in low to medium grade shear zones: A study from the Cap de Creus peninsula, NE Spain: Journal of Structural Geology, v. 24, p. 25–44, doi:10.1016/S0191-8141(01)00045-1.

Pryer, L.L., 1993, Microstructures in feldspars from a major crustal thrust zone—The Grenville Front, Ontario, Canada: Journal of Structural Geology, v. 15, p. 21–36, doi:10.1016/0191-8141(93)90076-M.

Pryer, L.L., and Robin, P., 1995, Retrograde metamorphic reactions in deforming granites and the origin of flame perthite: Journal of Metamorphic Geology, v. 13, no. 6, p. 645–658, doi:10.1111/j.1525-1314.1995.tb00249.x.

Rattenbury, M.S., 1991, The Fraser complex—High grade metamorphic, igneous and mylonitic rocks in central Westland, New Zealand: New Zealand Journal of Geology and Geophysics, v. 34, p. 23–33, doi:10.1080/00288306.1991.9514436.

Reed, J., 1964, Mylonites, cataclasites, and associated rocks along the Alpine fault, South Island, New Zealand: New Zealand Journal of Geology and Geophysics, v. 7, p. 645–684.

Rowe, C., Meneghini, F., and Moore, J., 2011, Textural record of the seismic cycle: Strain-rate variation in an ancient subduction thrust, *in* Fagereng, A., Toy, V.G., and Rowland, J., eds., Geology of the Earthquake Source: London, Geological Society of London, p. 77–95.

Sammis, C., Ozborne, R.H., Anderson, J.L., Banerdt, M., and White, P., 1986, Self-similar cataclasis in the formation of fault gouge: Pure and Applied Geophysics, v. 124, no. 1-2, p. 53–78, doi:10.1007/BF00875719.

Sandwell, D.T., and Smith, W.H.F., 1997, Marine gravity anomaly from Geosat and ERS 1 satellite altimetry: Journal of Geophysical Research, v. 102, no. B5, p. 10,039–10,054, doi:10.1029/96JB03223.

Schleicher, A.M., Sutherland, R., Townend, J., Toy, V., and van der Pluijm, B., 2015, Clay mineral formation and fabric development in the DFDP-1B borehole, central Alpine fault, New Zealand: New Zealand Journal of Geology and Geophysics, doi:10.1080/00288306.2014.979841 (in press).

Sibson, R.H., 1975, Generation of pseudotachylyte by ancient seismic faulting: Geophysical Journal of the Royal Astronomical Society, v. 43, p. 775–794, doi:10.1111/j.1365-246X.1975.tb06195.x.

Sibson, R.H., 1977, Fault rocks and fault mechanisms: Journal of the Geological Society of London, v. 133, p. 191–213, doi:10.1144/gsjgs.133.3.0191.

Sibson, R.H., and Toy, V.G., 2006, The habitat of fault-generated pseudotachylyte: Presence vs. absence of friction melt, *in* Abercrombie, R., McGarr, A., Di Toro, G., and Kanamori, H., eds., Earthquakes: Radiated Energy and the Physics of Faulting: American Geophysical Union Geophysical Monograph 170, p. 153–166.

Sibson, R.H., White, S.H., and Atkinson, B.K., 1979, Fault rock distribution and structure within the Alpine fault zone: A preliminary account, *in* Walcott, R.I., and Cresswell, M.M., eds., The Origin of the Southern Alps: Royal Society of New Zealand Bulletin 18, p. 55–65.

Sibson, R.H., White, S.H., and Atkinson, B.K., 1981, Structure and distribution of fault rocks in the Alpine fault zone, New Zealand, *in* McClay, K.R., and Price, N.J., eds., Thrust and Nappe Tectonics: London, Geological Society of London, p. 197–210.

Stöckhert, B., Brix, M.R., Kleinschrodt, R., Hurford, A.J., and Wirth, R., 1999, Thermochronometry and microstructures of quartz—A comparison with experimental flow laws and predictions on the temperature of the brittle-plastic transition: Journal of Structural Geology, v. 21, p. 351–369, doi:10.1016/S0191-8141(98)00114-X.

Sutherland, R., 1996, Transpressional development of the Australia-Pacific boundary through southern South Island, New Zealand: Constraints from Miocene–Pliocene sediments, Waiho-1 borehole, South Westland: New Zealand Journal of Geology and Geophysics, v. 39, p. 251–264, doi:10.1080/00288306.1996.9514709.

Sutherland, R., Eberhart-Phillips, D., Harris, R.A., Stern, T., Beavan, J., Ellis, S., Henrys, S., Cox, S., Norris, R.J., Berryman, K.R., Townend, J., Bannister, S., Pettinga, J., Leitner, B., Wallace, L., Little, T.A., Cooper, A.F., Yetton, M., and Stirling, M., 2007, Do great earthquakes occur on the Alpine fault in central South Island, New Zealand?, *in* Okaya, D., Stern, T.A., and Davey, F., eds., A Continental Plate Boundary: Tectonics at South Island, New Zealand: American Geophysical Union Geophysical Monograph 175, p. 235–251.

Sutherland, R., Toy, V., Townend, J., Eccles, J., Prior, D.J., Norris, R.J., Mariani, E., Faulkner, D.R., de Pascale, G., Carpenter, B.M., Boulton, C., Menzies, C.D., Cox, S.C., Little, T.A., Hasting, M., Cole-Baker, J.R., Langridge, R.M., Scott, H.R., Lindroos, Z.R., Fleming, B., and Wing, R., 2011, Operations and Well Completion Report for Boreholes DFDP-1A and DFDP-1B, Deep Fault Drilling Project, Alpine Fault, Gaunt Creek, New Zealand: GNS Science Report 2011/48, 99 p.

Sutherland, R., Toy, V.G., Townend, J., Cox, S.C., Eccles, J.D., Faulkner, D.R., Prior, D.J., Norris, R.J., Mariani, E., Boulton, C., Carpenter, B.M., Menzies, C.D., Little, T.A., Hasting, M., De Pascale, G.P., Langridge, R.M., Scott, H.R., Reid Lindroos, Z., Fleming, B., and Kopf, A.J., 2012, Drilling reveals fluid control on architecture and rupture of the Alpine fault, New Zealand: Geology, v. 40, p. 1143–1146, doi:10.1130/G33614.1.

Townend, J., 1999, Heat flow through the West Coast, South Island, New Zealand: New Zealand Journal of Geology and Geophysics, v. 42, p. 21–31, doi:10.1080/00288306.1999.9514829.

Townend, J., Sutherland, R., and Toy, V.G., 2009, Deep Fault Drilling Project—Alpine fault, New Zealand: Scientific Drilling, v. 8, p. 75–82, doi:10.5194/sd-8-75-2009.

Townend, J., Sutherland, R., Toy, V.G., Eccles, J.D., Boulton, C., Cox, S.C., and McNamara, D., 2013, Late-interseismic state of a continental plate–bounding fault: Petrophysical results from DFDP-1 wireline logging and core analysis, Alpine fault, New Zealand: Geochemistry Geophysics Geosystems, v. 14, no. 9, p. 3801–3820, doi:10.1002/ggge.20236.

Toy, V.G., 2008, Rheology of the Alpine Fault Mylonite Zone: Deformation Processes At and Below the Base of the Seismogenic Zone in a Major Plate Boundary Shear Zone [Ph.D. thesis]: Dunedin, New Zealand, University of Otago, 629 p. Retrieved from http://hdl.handle.net/10523/4548.

Toy, V.G., and Mitchell, T.M., 2014, Photograph of the month: Journal of Structural Geology, v. 64, no. 1, p. iii, doi:10.1016/SO191-8141(14)00094-7.

Toy, V.G., Prior, D.J., and Norris, R.J., 2008, Quartz fabrics in the Alpine fault mylonites: Influence of pre-existing preferred orientations on fabric development during progressive uplift: Journal of Structural Geology, v. 30, p. 602–621, doi:10.1016/j.jsg.2008.01.001.

Toy, V.G., Craw, D., Cooper, A.F., and Norris, R.J., 2010, Thermal regime in the central Alpine fault zone, New Zealand: Constraints from microstructures, biotite chemistry and fluid inclusion data: Tectonophysics, v. 485, p. 178–192, doi:10.1016/j.tecto.2009.12.013.

Toy, V.G., Ritchie, S., and Sibson, R.H., 2011, Diverse habitats of pseudotachylytes in the Alpine fault zone and relationships to current seismicity, *in* Fagereng, Å, Toy, V.G., and Rowland, J.V., eds., Geology of the Earthquake Source: A Volume in Honour of Rick Sibson: Geological Society of London Special Publication 359, p. 115–133, doi:10.1144/SP359.7.

Toy, V.G., Prior, D.J., Norris, R.J., Cooper, A.F., and Walrond, M., 2012, Relationships between kinematic indicators and strain during syn-deformational exhumation of an oblique slip, transpressive, plate boundary shear zone: The Alpine fault, New Zealand: Earth and Planetary Science Letters, v. 333-334, p. 282–292, doi:10.1016/j.epsl.2012.04.037.

Toy, V.G., Norris, R.J., Prior, D.J., Walrond, M., and Cooper, A.F., 2013, How do lineations reflect the strain history of transpressive shear zones? The example of the active Alpine fault zone, New Zealand: Journal of Structural Geology, v. 50, no. C, p. 187–198, doi:10.1016/j.jsg.2012.06.006.

Tullis, J., 2002, Deformation of granitic rocks: Experimental studies and natural examples: Reviews in Mineralogy and Geochemistry, v. 51, p. 51–95, doi:10.2138/gsrmg.51.1.51.

Tulloch, A., 1988, Batholiths, plutons, and suites: Nomenclature for granitoid rocks of Westland—Nelson, New Zealand: New Zealand Journal of Geology and Geophysics, v. 31, p. 505–509, doi:10.1080/00288306.1988.10422147.

Voll, G., 1976, Recrystallisation of quartz, biotite and feldspars from Erstfeld to the Leventina nappe, Swiss Alps, and its geological significance: Schweizerische Mineralogische und Petrographische Mitteilungen, v. 56, p. 641–647.

Warr, L.N., and Cox, S.C., 2001, Clay mineral transformations and weakening mechanisms along the Alpine fault, New Zealand, *in* Holdsworth, R.E., Strachan, R.A., Magloughlin, J.F., and Knipe, R.J., eds., The Nature and Tectonic Significance of Fault Zone Weakening: Geological Society of London Special Publication 186, p. 85–101, doi:10.1144/GSL.SP.2001.186.01.06.

Wells, A., Yetton, M.D., Duncan, R.P., and Stewart, G.H., 1999, Prehistoric dates of the most recent Alpine fault earthquakes, New Zealand: Geology, v. 27, p. 995–998, doi:10.1130/0091-7613(1999)027<0995:PDOTMR>2.3.CO;2.

Whitney, D.L., and Evans, B.W., 2010, Abbreviations for names of common rock-forming minerals: The American Mineralogist, v. 95, p. 185–187, doi:10.2138/am.2010.3371.

Wibberley, C.A.J., and Shimamoto, T., 2003, Internal structure and permeability of major strike-slip fault zones: The Median Tectonic Line in Mie Prefecture, southwest Japan: Journal of Structural Geology, v. 25, p. 59–78, doi:10.1016/S0191-8141(02)00014-7.

Woodcock, N.H., and Mort, K., 2008, Classification of fault breccias and related fault rocks: Geological Magazine, v. 145, no. 03, p. 435–440, doi:10.1017/S0016756808004883.

MANUSCRIPT RECEIVED 18 MAY 2014
REVISED MANUSCRIPT RECEIVED 28 NOVEMBER 2014
MANUSCRIPT ACCEPTED 16 JANUARY 2015

Printed in the USA